

This discussion paper is/has been under review for the journal Atmospheric Measurement Techniques (AMT). Please refer to the corresponding final paper in AMT if available.

# A two-channel, Thermal Dissociation Cavity-Ringdown Spectrometer for the detection of ambient NO<sub>2</sub>, RO<sub>2</sub>NO<sub>2</sub> and RONO<sub>2</sub>

J. Thieser<sup>1</sup>, G. Schuster<sup>1</sup>, G. J. Phillips<sup>1,a</sup>, A. Reiffs<sup>1</sup>, U. Parchatka<sup>1</sup>, D. Pöhler<sup>2</sup>, J. Lelieveld<sup>1</sup>, and J. N. Crowley<sup>1</sup>

<sup>1</sup>Max-Planck-Institut für Chemie, Division of Atmospheric Chemistry, Mainz, Germany

<sup>2</sup>Institute of Environmental Physics, University of Heidelberg, Heidelberg, Germany

<sup>a</sup>now at: Department of Natural Sciences, University of Chester, Chester, UK

Received: 23 September 2015 – Accepted: 8 October 2015 – Published: 3 November 2015

Correspondence to: J. N. Crowley (john.crowley@mpic.de)

Published by Copernicus Publications on behalf of the European Geosciences Union.

Title Page

Abstract

Introduction

Conclusions

References

Tables

Figures

◀

▶

◀

▶

Back

Close

Full Screen / Esc

Printer-friendly Version

Interactive Discussion



## Abstract

We describe a Thermal Dissociation Cavity-Ring-Down Spectrometer (TD-CRDS) for measurement of ambient NO<sub>2</sub>, total peroxy nitrates (ΣPNs) and total alkyl nitrates (ΣANs). The spectrometer has two separate cavities operating at ~ 405.2 and 408.5 nm, one cavity (reference) samples NO<sub>2</sub> continuously from an inlet at ambient temperature, the other samples sequentially from an inlet at 473 K in which PN<sub>s</sub> are converted to NO<sub>2</sub> or from an inlet at 723 K in which both PN<sub>s</sub> and AN<sub>s</sub> are converted to NO<sub>2</sub>, difference signals being used to derive mixing ratios of ΣPN<sub>s</sub> and ΣAN<sub>s</sub>. We describe an extensive set of laboratory experiments and numerical simulations to characterise the fate of organic radicals in the hot inlets and cavity and derive correction factors to account for the bias resulting from interaction of peroxy radicals with ambient NO and NO<sub>2</sub>. Finally, we present the first measurements and comparison with other instruments during a field campaign, outline the limitations of the present instrument and provide an outlook for future improvements.

## 1 Introduction

Reactive nitrogen oxides are centrally important trace gases in atmospheric chemistry as they affect air quality, climate, and ecosystem nutrient. Nitrogen oxides are involved in the photochemical production/loss of ozone (O<sub>3</sub>), they interact with HO<sub>x</sub> radicals (HO<sub>x</sub> ≡ OH + HO<sub>2</sub> + RO<sub>2</sub>, where R is an organic fragment) to either catalyse ozone formation or terminate the HO<sub>x</sub> catalytic chain and thereby suppress ozone formation. Nitrogen oxides are largely emitted to the atmosphere as NO which is then oxidised to NO<sub>2</sub>. Beside inorganic NO<sub>x</sub> (NO<sub>x</sub> ≡ NO + NO<sub>2</sub>) there are several classes of organic nitrogen oxides including peroxy nitrates (RO<sub>2</sub>NO<sub>2</sub>) and alkyl nitrates (RONO<sub>2</sub>) which have an important influence on atmospheric composition. Peroxy nitrates and alkyl nitrates are produced as by-products in the photochemical oxidation of volatile organic compounds (VOCs) in the presence of NO<sub>x</sub>, the same processes and reactions that

Title Page

Abstract

Introduction

Conclusions

References

Tables

Figures



Back

Close

Full Screen / Esc

Printer-friendly Version

Interactive Discussion



produce the pollutant and greenhouse gas ozone. In addition to being indicators of photochemical ozone production, organic nitrates exert a direct influence on regional ozone levels and can have a large impact on the global distribution of  $\text{NO}_x$  and thus ozone (Roberts, 1990; Singh and Hanst, 1981).

5 Peroxy nitrates are formed in the reaction of  $\text{RO}_2$  with  $\text{NO}_2$  Reaction (R1) and their lifetime with respect to thermal decomposition Reaction (R2) is strongly temperature dependent.



10 Peroxy nitrates such as peroxyacetic nitric anhydride (PAN,  $\text{CH}_3\text{C}(\text{O})\text{O}_2\text{NO}_2$ ), which possess an acyl group adjacent to the peroxy group have thermal decomposition lifetimes that vary from less than an hour at the surface at temperatures close to 295 K, to more than a month at the low temperature of e.g. the upper troposphere. Consequently peroxyacetic nitric anhydrides are important reservoirs of  $\text{NO}_x$  and mediators of its  
15 long-range transport to remote regions. In contrast, peroxy nitrates that do not possess the acyl group (e.g.  $\text{HO}_2\text{NO}_2$  or  $\text{CH}_3\text{O}_2\text{NO}_2$ ) are much shorter lived and are only found in significant abundance in cold regions of the troposphere such as in the Antarctic boundary layer (Slusher et al., 2002) and the upper troposphere (Browne et al., 2011). Other losses of  $\text{RO}_2\text{NO}_2$  such as photolysis or reaction with OH are vastly reduced  
20 in importance compared to thermal decomposition (Talukdar et al., 1995). Throughout this manuscript, we use the term “PN” to refer to peroxy nitrates.

During daytime, alkyl nitrates ( $\text{RONO}_2$ ) are formed in a minor branch of the reaction between organic peroxy radicals ( $\text{RO}_2$ ) and NO (Reaction R3). The dominant reaction channel (Reaction R4) leads to the formation of  $\text{NO}_2$  and therefore (via its photolysis)  
25 to ozone.

**TD-CRDS for  $\text{NO}_2$ ,  
 $\text{RO}_2\text{NO}_2$  and  $\text{RONO}_2$** 

J. Thieser et al.

Title Page

Abstract

Introduction

Conclusions

References

Tables

Figures

◀

▶

◀

▶

Back

Close

Full Screen / Esc

Printer-friendly Version

Interactive Discussion



The fractional flux through Reaction (R3) (relative to Reactions R3 and R4) depends on the carbon chain and also the pressure and temperature and can vary from very low values (< 2 %) for small hydrocarbons to > 50 % for longer chain hydrocarbons such as heptane (Lee et al., 2014).

5 Alkyl nitrates can also be formed at night in the NO<sub>3</sub> induced degradation of unsaturated VOCs, which proceeds via addition of NO<sub>3</sub> across the double bond to form (in the presence of O<sub>2</sub>) a nitrooxyalkyl peroxy radical that can further react to form an alkyl nitrate with e.g. hydroxyl- or carbonyl groups:



10 Yields of ANs from these reactions can be large, especially for biogenic organics such as isoprene or terpenes (Atkinson and Arey, 2003). Hereafter, we use the term “AN” to refer to alkyl nitrates, irrespective of their mode of generation.

15 ANs which do not contain double bonds or hydroxyl groups generally have a low affinity for surfaces and react only slowly with oxidants such as OH (Talukdar et al., 1997) so that they can sequester a significant fraction of reactive nitrogen (Perring et al., 2013).

20 The organic nitrate content of ambient air comprises a mixture of many structurally distinct compounds in generally low individual abundance, which makes their quantitative determination challenging. Organic nitrates have been measured on many occasions using gas chromatography (GC). The advantage of this technique is a limit of detection of a few pptv and the possibility to distinguish between individual organic nitrates (see e.g. Roberts et al., 2003). The disadvantages are the requirement of calibration for many trace gases (usually not commercially available) and low time resolution (Hao et al., 1994; Flocke et al., 2005). Recently, PAN and other peroxyacetylic nitric anhydrides such as MPAN (peroxymethacrylic nitric anhydride) and PPAN (peroxypropionic nitric anhydride) have been identified and measured with sub-second time resolution using thermal dissociation chemical ionisation mass spectrometry (TD-CIMS) (Phillips

Title Page

Abstract

Introduction

Conclusions

References

Tables

Figures



Back

Close

Full Screen / Esc

Printer-friendly Version

Interactive Discussion



et al., 2013; LaFranchi et al., 2009; Roiger et al., 2011; Mielke and Osthoff, 2012; Zheng et al., 2011; Wolfe et al., 2009).

The first measurements of alkyl nitrates in the atmosphere were made by Atlas et al. (1988), and subsequent calculations and measurements suggested that the atmosphere should contain a wide suite of individual alkyl and multifunctional nitrates (Atherton and Penner, 1988; Calvert and Madronich, 1987; Schneider and Ballschmiter, 1999) and that hydroxy alkyl nitrates derived from isoprene oxidation could constitute as much as 12–26 % of tropospheric  $\text{NO}_y$  (Trainer et al., 1991). Total measured  $\text{NO}_y$  has frequently been found to exceed the sums of different nitrogen compounds ( $\text{NO} + \text{NO}_2 + \text{PAN} + \text{HNO}_3 + \text{HONO} + \text{NO}_3 + 2\text{N}_2\text{O}_5 + \dots$ ), the range of the “missing”  $\text{NO}_y$  being 10–20 %. In most of these observations the total alkyl nitrate content was not measured or only partially (e.g. Buhr et al., 1990; Fahey et al., 1986; Parrish and Buhr, 1993; Ridley et al., 1990; Williams et al., 1997; Singh et al., 1996).

These considerations led to the development of instruments (Day et al., 2002) which make use of the thermal instability of  $\text{RO}_2\text{NO}_2$  and  $\text{RONO}_2$  at elevated temperatures and which report measurements of the sum of peroxy nitrates ( $\Sigma\text{PN}$ ) or the sum of alkyl-nitrates ( $\Sigma\text{AN}$ ) by monitoring the  $\text{NO}_2$  product of the thermal decomposition of PNs and ANs to  $\text{NO}_2$  at different temperatures.



These studies have helped to confirm that ANs and PNs represent a significant fraction of atmospheric  $\text{NO}_y$  and confirm their role in e.g.  $\text{HO}_x$  radical chain termination, or as indicators of photochemical  $\text{O}_3$  generation (see e.g. Perring et al., 2013; Rosen et al., 2004; Day et al., 2003).

Here we describe a recently constructed instrument to measure ambient  $\text{NO}_2$  and also that formed from the thermal decomposition of ANs and PNs via cavity-ring-down spectroscopy.

## TD-CRDS for $\text{NO}_2$ , $\text{RO}_2\text{NO}_2$ and $\text{RONO}_2$

J. Thieser et al.

Title Page

Abstract

Introduction

Conclusions

References

Tables

Figures

◀

▶

◀

▶

Back

Close

Full Screen / Esc

Printer-friendly Version

Interactive Discussion



## 2 Principal of operation and instrument set-up

Cavity-ring-down spectroscopy (hereafter CRDS) and its use for the sensitive detection of atmospheric trace gases has been reviewed in detail (Brown, 2003; Berden et al., 2000). CRDS is based on direct absorption spectroscopy in which the absorption path length is enhanced by a high finesse cavity formed by a set of two highly reflective mirrors. Most applications use pulsed or intensity modulated CW lasers as light source with direct coupling into the cavity via one (front) mirror. The present experiment uses a square-wave, on/off modulated CW laser. During the “laser-on” phase the light intensity in the cavity builds up to a level determined by mirror reflectivity and transmission. The light leaking out through the back mirror during “laser off” mode is analysed to derive an exponential decay constant, which is reduced in the presence of an absorbing or scattering gas. This provides an absolute measurement of optical extinction, as given in Eq. (1).

$$\sigma[A] = \alpha = \frac{l}{cd} \left( \frac{1}{\tau} - \frac{1}{\tau_0} \right) \quad (1)$$

where,  $\sigma$  is the absorption cross section of the absorber, averaged over the laser spectrum,  $[A]$  is the concentration of the absorber,  $\alpha$  is the optical extinction coefficient (units of inverse length),  $c$  is the speed of light,  $\tau$  and  $\tau_0$  are the exponential decay constants with and without the absorber in the cavity and  $l/d$  is the ratio of the length over which the absorber is present to the distance between the two resonator mirrors. In order to derive  $\tau_0$  the cavity is flushed with zero air (see later).

Essential features of the TD-CRDS instrument described here are displayed in Fig. 1. Our two-channel CRDS utilises two laser diodes (Lasercomponents, optical power: 120 mW) in commercially available laser diode heads (Thorlabs) with current- and temperature controller units (Thorlabs ITC 510 and ITC 502). The lasers are modulated on and off at 1666 Hz (duty cycle 50 %) by a 6 V square-wave signal. The rise and fall time of the intensity is less than 1  $\mu$ s, which, under normal conditions ( $\text{NO}_2 < 1$  ppm) is rapid on the time scale of the decay of intensity from the optical cavities. Optical

Title Page

Abstract

Introduction

Conclusions

References

Tables

Figures



Back

Close

Full Screen / Esc

Printer-friendly Version

Interactive Discussion





is repeated 32 times, resulting in a time resolution of about 4 s per data point for both channels.

The two-channel CRDS consists of two nominally identical cavities (both thermostated to 308 K) and sample inlets. The cavities are made of 10 mm i.d. Duran glass, which was coated with a thin film of Teflon (DuPont, FEP TE9568) to minimise interaction of traces gases with the walls, which could potentially results in loss or production of NO<sub>2</sub>. Aerosols are prevented from entering the inlets and cavities using a 47 mm diameter, 2 µm PTFE filter (PAL Teflo).

The cavities are operated at sub-ambient pressure (typically 800–850 mbar) which is held constant using an additional, mass flow controlled branch linking the inlet manifold to a pump. This line also contains a relative humidity and temperature sensor to enable corrections for laser light scattering by H<sub>2</sub>O vapour to be made (see later). Ambient air enters the centre of the cavities at a flow rate of 2.0 standard litres per minute in each channel, resulting in a cavity residence time of about 1.2 s. However, as concentrations are integrated over the entire cavity length the average residence time of a molecule of NO<sub>2</sub> detected in the cavity will be less than this.

Values of  $\tau_0$  were obtained at regular intervals (every 5–10 min) by switching ambient air for zero-air for a short period (1–2 min). 3-way Teflon valves (NRResearch) which have been shown not to permanently remove PNs, ANs or NO<sub>2</sub> were used. This frequency of zeroing was found to be sufficient to track drifts in the ring down constant (see later).

One of the cavities (reference cavity in Fig. 1) continuously measures ambient NO<sub>2</sub>, the second cavity (TD-cavity) samples alternatively from three separate, quartz tubes of i.d. 1.5 cm and length 42 cm. 15 cm sections of two of the quartz tubes were placed in commercial ovens (Carbolite) and heated up to 473 and 723 K, whereby these are oven temperatures and do not necessarily reflect the temperature of gas flowing through the quartz tubing. The cavity attached to the heated quartz inlets thus measures the sum of NO<sub>2</sub> plus NO<sub>2</sub> generated from the thermal dissociation of organic nitrates. We refer to the NO<sub>2</sub> measurements when sampling from these inlets as [NO<sub>2</sub>]<sub>ref</sub>, [NO<sub>2</sub>]<sub>TD</sub>, [NO<sub>2</sub>]<sub>TD 473</sub>, and [NO<sub>2</sub>]<sub>TD 723</sub>.

TD-CRDS for NO<sub>2</sub>,  
RO<sub>2</sub>NO<sub>2</sub> and RONO<sub>2</sub>

J. Thieser et al.

Title Page

Abstract

Introduction

Conclusions

References

Tables

Figures



Back

Close

Full Screen / Esc

Printer-friendly Version

Interactive Discussion







600 pptv) is given in Fig. SI 2. In this case, PAN was calculated by multiplying the NO mixing ratio (itself calculated from the manufacturer's specification and dilution factors) by 1.1. In this range of PAN mixing ratios, the response of the TD-CRDS to various NO (and thus PAN) concentrations is linear, with a gradient close to unity, suggesting that PAN detection as NO<sub>2</sub> is quantitative in our TD-CRDS.

Samples of alkyl nitrates in air of known concentrations (~ 3 and ~ 6 ppb) were prepared manometrically and used to derive the stoichiometry of conversion of 2-propyl nitrate to NO<sub>2</sub>. The results are also displayed in Fig. SI 2 and indicate that, at 723 K, 2-propyl nitrate in air is quantitatively converted to NO<sub>2</sub>. Later we discuss the effects of non-stoichiometric conversion of PAN and ANs to NO<sub>2</sub> due to reactions of the organic radical fragment formed during thermal dissociation.

A typical measurement sequence (in this case with an ambient air sample) is illustrated in Fig. 4 which displays NO<sub>2</sub> mixing ratios in both cavities. The black data points are NO<sub>2</sub> measurements in the reference cavity, the blue and red data points were obtained when the TD cavity was sampling from the 723 and 473 K ovens, respectively. The green data points were obtained in the TD-cavity when the gas was sampled via the bypass and serve as a check for consistency between the two cavities. The gaps in the data are zeroing periods when the inlet was filled with synthetic air. Zeroing was conducted at the same pressure as the measurement to avoid changes in ring-down due to changes in Rayleigh scattering by air. Note that the change in ring-down time at 405 nm caused by a 3.3 mbar change in pressure of air is the equivalent of ~ 100 pptv of NO<sub>2</sub>. As we discuss later, the use of dry zero-air to derive  $\tau_0$  also requires correction for the difference in scattering cross section of dry and humid (i.e. ambient) air. Experiments to derive correction factors for this effect are described in Sect. 2.1.

Subtraction of the NO<sub>2</sub> mixing ratio measured when sampling from the reference cavity ( $[\text{NO}_2]_{\text{ref}}$ ) from that obtained in the cavity sampling from the 473 K inlet ( $[\text{NO}_2]_{\text{TD473}}$ ) in principal yields the summed mixing ratio of PNs that decompose thermally at this temperature. The main contributor will usually be CH<sub>3</sub>C(O)O<sub>2</sub>NO<sub>2</sub> (PAN), with contributions from larger PNs and other NO<sub>2</sub>-containing trace gases (e.g. N<sub>2</sub>O<sub>5</sub>, see later)

TD-CRDS for NO<sub>2</sub>, RO<sub>2</sub>NO<sub>2</sub> and RONO<sub>2</sub>

J. Thieser et al.

Title Page

Abstract

Introduction

Conclusions

References

Tables

Figures



Back

Close

Full Screen / Esc

Printer-friendly Version

Interactive Discussion



TD-CRDS for NO<sub>2</sub>,  
RO<sub>2</sub>NO<sub>2</sub> and RONO<sub>2</sub>

J. Thieser et al.

Title Page

Abstract

Introduction

Conclusions

References

Tables

Figures

◀

▶

◀

▶

Back

Close

Full Screen / Esc

Printer-friendly Version

Interactive Discussion



which also readily decompose at this temperature. In order to derive the  $\Sigma$ ANs mixing ratio we first have to interpolate  $[\text{NO}_2]_{\text{TD}473}$  (red data points) and then subtract this from  $[\text{NO}_2]_{\text{TD}723}$  (blue data points). The need to interpolate the data from the 473 K channel means that the accuracy of the  $\Sigma$ ANs measurement is impacted by variability of the  $\Sigma$ PNs mixing ratio.

## 2.1 Data corrections

### 2.1.1 $l$ to $d$ ratio

Owing to the use of purge gas flows at the mirrors, the physical distance between the mirrors ( $d$ ) is longer than the length through which optical absorption takes place ( $l$ ). The ratio of  $d$  to  $l$  was obtained by flowing a constant amount of NO<sub>2</sub>/N<sub>2</sub> through the cavity and varying the purge gas flow from zero to 500 sccm as shown previously for our red-laser instrument for measuring NO<sub>3</sub> and N<sub>2</sub>O<sub>5</sub> (Schuster et al., 2009). The reduction in NO<sub>2</sub> signal at a purge gas flow of 100 sccm compared to when the complete volume between the mirrors was flushed with NO<sub>2</sub> (no mirror purge) was 5 %, indicating a  $d$  to  $l$  ratio of 1.06.

### 2.1.2 Inlet and filter loss of NO<sub>2</sub>, PNs and ANs

The inlet transmission and filter losses were investigated in the laboratory for NO<sub>2</sub>,  $\Sigma$ PNs and  $\Sigma$ ANs. The response to concentration changes was nearly instantaneous, suggesting that wall losses or associated memory effects on the inlet and cavity tubing are insignificant. Transmission through a fresh PTFE filter (2  $\mu\text{m}$  pore size) housed in a PFA filter holder was, within measurement precision, quantitative. Daily replacement when sampling ambient air was found to be sufficient to maintain this high transmission.

### 2.1.3 Relative humidity

Use of dry, zero-air to derive  $\tau_0$  requires correction for the fact that the Rayleigh scattering cross section of water vapour is smaller than that of dry air. The size of this effect was investigated in the laboratory by comparing  $\tau_0$  (obtained in dry, zero-air) to  $\tau$  in zero-air at various relative humidities (RH) between 10 and 70 % (Delta Ohm, HD49T) at room temperature. The results are displayed in Fig. 5 which, at constant total pressure, shows a linear decrease in extinction with increasing water vapour concentration. This confirms that, in contrast to the conclusions of Hargrove and Zhang (2008) who found a large, positive interference caused by water vapour at 405 nm, the effect of H<sub>2</sub>O in ambient air is to reduce extinction due to its lower Rayleigh scattering cross section. The slope of the fit in Fig. 5 yields a cross section difference between water vapour and dry air of  $\Delta\sigma_{\text{Rayleigh}}^{405-409\text{ nm}} = (-4.0 \pm 0.4) \times 10^{-27} \text{ cm}^2 \text{ molecule}^{-1}$ . This is somewhat lower than the value of  $\Delta\sigma_{\text{Rayleigh}}^{405-409\text{ nm}} = (-5.0 \pm 0.2) \times 10^{-27} \text{ cm}^2 \text{ molecule}^{-1}$  obtained at  $404 \pm 0.5 \text{ nm}$  by Fuchs et al. (2009). To put this in context, the correction applied for an ambient relative humidity of 70 % at 22 °C is equivalent to 130 pptv NO<sub>2</sub> under normal operating conditions. At low NO<sub>2</sub> mixing ratios the correction is therefore large (e.g. 100 % at 100 pptv). We discuss the impact of this later when assessing the total uncertainty.

### 2.1.4 Presence of NO<sub>2</sub> in zero air

The presence of NO<sub>2</sub> in the zero air used would lead to an underestimation of the ambient NO<sub>2</sub> concentrations. In order to check for NO<sub>2</sub> impurity in bottled zero air (hydrocarbon free) we constructed and characterised an efficient, all-quartz blue-light converter (BLC) (Kley and McFarland, 1980) to remove NO<sub>2</sub>. The BLC consisted of a thin (ID 10 mm) quartz tube of ~ 30 cm length with the light from two LED arrays operating at a central wavelength of ~ 390 nm coupled into the tube via quartz end-windows. NO<sub>2</sub> entered and exited the BLC via side-arms located close to the end-windows and, at

[Title Page](#)[Abstract](#)[Introduction](#)[Conclusions](#)[References](#)[Tables](#)[Figures](#)[Back](#)[Close](#)[Full Screen / Esc](#)[Printer-friendly Version](#)[Interactive Discussion](#)

Title Page

Abstract

Introduction

Conclusions

References

Tables

Figures



Back

Close

Full Screen / Esc

Printer-friendly Version

Interactive Discussion



a flow rate of 1 SLM, was removed with an efficiency of ~ 60 %, independent of NO<sub>2</sub> mixing ratios up to about 1 ppb. The use of quartz rather than Teflon for the construction of the BLC reduces memory effects related to NO<sub>2</sub> degassing from or being formed on UV-illuminated Teflon surfaces. The level of NO<sub>2</sub> in the zero air could thus be monitored with the CRDS by flowing the air through the BLC and modulating the light on-and-off over several 1 min cycles. In all bottles tested during a field campaign (PARADE, see below) no change in NO<sub>2</sub> signal was observed, placing an upper limit of about 20 pptv of NO<sub>2</sub> in the zero-air, implying a maximum bias of –20 pptv in the NO<sub>2</sub> measurements.

### 2.1.5 Formation of NO<sub>2</sub> via O<sub>3</sub> + NO

Common to several established instruments that measure NO<sub>2</sub>, its formation in a dark reaction between NO and O<sub>3</sub> in e.g. an inlet line has to be considered (Ryerson et al., 2000).



Laboratory experiments were thus conducted to examine the formation of NO<sub>2</sub> via the reaction of O<sub>3</sub> with NO, with the mixing ratios of NO (0–10 ppbv) and O<sub>3</sub> (25, 48 or 80 ppbv) varied systematically. NO was taken from a bottled standard, O<sub>3</sub> was formed by passing synthetic air over a pen-ray lamp and its concentration was monitored using a photometric O<sub>3</sub> analyser (Thermo Environmental Instruments, model 49).

Under conditions of low conversion of NO and O<sub>3</sub>, the amount of NO<sub>2</sub> formed [NO<sub>2</sub>]<sub>t</sub> can be calculated from the initial concentrations of NO and O<sub>3</sub> and the reaction time (*t*): [NO<sub>2</sub>]<sub>t</sub> = *k*<sub>8</sub>[NO][O<sub>3</sub>]*t*, where *k*<sub>8</sub> is the rate coefficient for Reaction (R8) and is given as 2.07 × 10<sup>–12</sup> exp(–1400/*T*) cm<sup>3</sup> molecule<sup>–1</sup> s<sup>–1</sup> (Atkinson et al., 2004) which results in a room temperature rate coefficient of about 1.9 × 10<sup>–14</sup> cm<sup>3</sup> molecule<sup>–1</sup> s<sup>–1</sup>. For the NO<sub>2</sub> reference channel (inlet at 298 K, cavity at 308 K) the amount of NO<sub>2</sub> formed was entirely consistent with the kinetic parameters and reaction time used. This is demonstrated in Fig. 6.

TD-CRDS for NO<sub>2</sub>,  
RO<sub>2</sub>NO<sub>2</sub> and RONO<sub>2</sub>

J. Thieser et al.

Title Page

Abstract

Introduction

Conclusions

References

Tables

Figures



Back

Close

Full Screen / Esc

Printer-friendly Version

Interactive Discussion



The expression above indicates that the rate coefficient increases significantly with temperature so that an increase in the formation of NO<sub>2</sub> would be expected in the ovens of the TD-cavity. Indeed, in order to explain the formation of NO<sub>2</sub> in the 473 and 723 K channels, “effective” rate coefficients of  $2.5 \times 10^{-14}$  and  $6.2 \times 10^{-14}$  cm<sup>3</sup> molecule<sup>-1</sup> s<sup>-1</sup> were necessary. These effective rate coefficients take into account the fact that the NO<sub>2</sub> production rate is time dependent owing to the temperature gradients through the apparatus and are thus appropriate for making corrections for NO<sub>2</sub> formed in this particular system. In order to illustrate the size of this correction we assume O<sub>3</sub> = 50 ppb, NO = 1 ppb, NO<sub>2</sub> = 5 ppb, which are typical of a semi-polluted environment during day-time. The amount of NO<sub>2</sub> formed in the reference (cold) channel via this route is 0.1 ppbv or 2 % of ambient NO<sub>2</sub>. This increases to 2.6 and 6.5 % in the 473 and 723 K channels, respectively.

### 2.1.6 Pyrolysis of O<sub>3</sub>

The potential for the reduction of NO<sub>2</sub> to NO via reaction with O(<sup>3</sup>P) atoms formed in the thermal degradation of O<sub>3</sub> has been discussed by Day et al. (2002) who show that it is of negligible importance for measurements of PNs and ANs conducted at the temperatures used here. As the equilibrium between O atoms and O<sub>3</sub> will be strongly shifted to O<sub>3</sub> in our experiments at higher pressure and partial pressures of O<sub>2</sub>, we can safely ignore the pyrolysis of O<sub>3</sub> as source of systematic error.

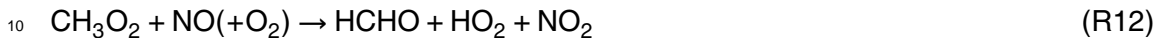
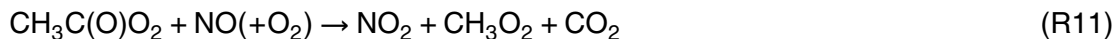
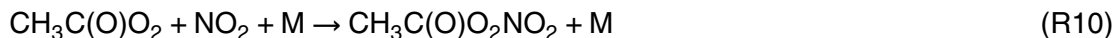
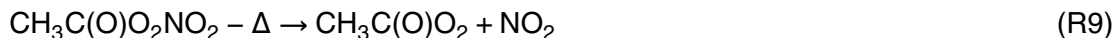
### 2.1.7 Reactions of organic radicals with NO and NO<sub>2</sub>

The method of thermal dissociation of PNs or ANs to NO<sub>2</sub> and subsequent monitoring of NO<sub>2</sub> requires knowledge of the stoichiometry of the conversion factor under operating conditions. As discussed already (Wooldridge et al., 2010; Day et al., 2002) deviation from an ideal conversion factor of unity occurs when the NO<sub>2</sub> formed in the thermal dissociation recombines with the organic radical, or when the organic radical

can react with other atmospheric substituents (such as NO) to form NO<sub>2</sub>. The reactions which take place in the 473 and 723 K inlets are discussed below:

### 473 K inlet:

Alkyl nitrates pass through the 473 K inlet without dissociation so we need only to consider the fate of PNs. For PAN (CH<sub>3</sub>C(O)O<sub>2</sub>NO<sub>2</sub>) the major reactions that either form or consume NO<sub>2</sub> are:



Note that Reactions (R11) and (R12) are composite reactions in which the initially formed CH<sub>3</sub>CO<sub>2</sub> (Reaction R11) and CH<sub>3</sub>O (Reaction R12) either decompose and/or react with O<sub>2</sub> to give the products listed.

Reaction (R10) results in underestimation of RO<sub>2</sub>NO<sub>2</sub> mixing ratios, whereas Reaction (R11) and subsequent Reactions (R12) and (R13) of organic radical fragments results in an overestimation by oxidizing a fraction of any ambient NO. These reactions compete with loss of the organic radical to the wall of the hot quartz tubing or their thermal decomposition so that the size of the artefact will depend non-linearly on ambient levels of NO and NO<sub>2</sub> as well as the concentration of RO<sub>2</sub>NO<sub>2</sub>. The reaction scheme above indicates that, when wall losses of the radicals are neglected, the presence of sufficient NO can result in the generation of three extra NO<sub>2</sub> for each one formed directly in PAN decomposition.

Such effects can be reduced by operating the instrument at very low pressures (and absolute trace gas concentrations) as described by the Berkeley group (Wooldridge

Title Page

Abstract

Introduction

Conclusions

References

Tables

Figures



Back

Close

Full Screen / Esc

Printer-friendly Version

Interactive Discussion



et al., 2010). As discussed by Paul et al. (2009), this option is not available for a CRDS instrument which generally operates at higher pressures in order to maintain sufficient sensitivity.

Initial observations of an unchanging mixing ratio when flowing samples of PAN or 2-propyl-nitrate at levels of 1–2 ppb through the inlet and cavities at flow rates of between 1 and 3 L (std) min<sup>-1</sup> (SLM) and thus varying the reaction time by a factor of three indicated that such effects are small, in accord with the observations of Paul et al. (2009) and the data shown in Fig. SI 2. A detailed experimental investigation of this artefact was conducted in a set of experiments in which known amounts of NO or NO<sub>2</sub> were added to a PAN sample (between 500 and 5000 pptv) and monitoring the resultant NO<sub>2</sub> formed by thermal decomposition.

The results of experiments in which various concentrations of NO<sub>2</sub> were added to three different concentrations of PAN are displayed in Fig. 7. In these experiments, PAN was supplied from a diffusion source of PAN in tridecane held at 273 K.

In the absence of recombination of CH<sub>3</sub>C(O)O<sub>2</sub> radicals and NO<sub>2</sub> the difference between [NO<sub>2</sub>]<sub>TD473</sub> and [NO<sub>2</sub>]<sub>ref</sub> (*y* axis) would be a flat line at the initial PAN concentration. The effect of reformation of PAN is clearly seen in the data, so that, at an initial concentration of about 700 pptv of PAN, only 460 pptv would be detected as [NO<sub>2</sub>]<sub>TD473</sub> – [NO<sub>2</sub>]<sub>ref</sub> if 8 ppb NO<sub>2</sub> were also present. Even in the absence of added NO<sub>2</sub>, [NO<sub>2</sub>]<sub>TD473</sub> – [NO<sub>2</sub>]<sub>ref</sub> is smaller than the amount of PAN added as some of the 700 pptv of the NO<sub>2</sub> formed in the thermal dissociation region can also recombine with CH<sub>3</sub>C(O)O<sub>2</sub>.

In Fig. 8 we display the results of a similar set of experiments in which NO was added instead of NO<sub>2</sub>. As expected from the reaction scheme above, by adding NO we convert CH<sub>3</sub>C(O)O<sub>2</sub> radicals into NO<sub>2</sub> and thus observe a positive bias in the [NO<sub>2</sub>]<sub>TD473</sub> – [NO<sub>2</sub>]<sub>ref</sub> signal. For an initial PAN concentration of about 1000 pptv, the result of adding 4 ppbv of NO is to overestimate the PAN concentration by about 180 %.

As ambient air contains NO and NO<sub>2</sub> in greatly varying amounts and ratios, there is no simple analytical expression that can provide a correction for the opposing effects

TD-CRDS for NO<sub>2</sub>,  
RO<sub>2</sub>NO<sub>2</sub> and RONO<sub>2</sub>

J. Thieser et al.

Title Page

Abstract

Introduction

Conclusions

References

Tables

Figures



Back

Close

Full Screen / Esc

Printer-friendly Version

Interactive Discussion





TD-CRDS for NO<sub>2</sub>,  
RO<sub>2</sub>NO<sub>2</sub> and RONO<sub>2</sub>

J. Thieser et al.

Title Page

Abstract

Introduction

Conclusions

References

Tables

Figures



Back

Close

Full Screen / Esc

Printer-friendly Version

Interactive Discussion



of PN underestimation due to NO<sub>2</sub> recombination or PN overestimation as a result of peroxy radical induced oxidation of ambient NO. The sign and size of the bias depends on the concentrations of PN, NO and NO<sub>2</sub> and also the rate of wall loss of the peroxy radicals involved (Wooldridge et al., 2010). In order to gain insight into the reactions taking place in the ovens and in the piping leading to the cavities and in the cavities themselves, we conducted a detailed set of numerical simulations (FACSIMILE, Curtis and Sweetenham, 1987) of the laboratory experiments described above.

The simulations were initialised with position dependent temperature gradients in the oven and subsequent piping and cavities, which were derived by inserting a thermocouple into the quartz tubing and measuring the temperature of the inner wall at different distances from the cold, front edge of the oven. As the 473 K oven and cavities were maintained at 800 mbar, the large variation in temperature results in significant gradients in the gas-density and flow velocity in hot and cold parts of the apparatus, which were also accounted for in the simulations. The gas-phase reactions accounted for in the chemical scheme are listed in the Supplement, the temperature dependent rate constants being taken mainly from IUPAC (IUPAC, 2015). The goal of the simulations was to mimic the observed dependence of the PN-NO<sub>2</sub> signals on the amounts of NO and NO<sub>2</sub> added (i.e. the data in Figs. 7 and 8).

Initial simulations confirmed that the bias due to adding NO and NO<sub>2</sub> was dependent on the assumed wall loss rate constant ( $k_{\text{wall}}$ ) of the HO and peroxy radicals. Simulations with unrealistically large wall loss rates such as to make all other radical reactions insignificant removed the bias completely and thus could not reproduce the observations. The use of very small (or zero) values of  $k_{\text{wall}}$  resulted in an overestimation of the bias. Although  $k_{\text{wall}}$  clearly plays a role in determining the size of the bias, the use of a single value of  $k_{\text{wall}}$  was not able to reproduce the observed effect for different initial PAN concentrations, with lower values of  $k_{\text{wall}}$  required for experiments in which PAN was large. This observation is consistent with the radicals being lost to the surface via a Langmuir–Hinshelwood type mechanism, in which the rates of surface reactions are

inversely dependent on radical densities, often described in terms of “surface passivation”.

The uptake coefficient ( $\gamma$ ) for a gas to a surface can be described by the following expression (Crowley et al., 2010a):

$$\frac{1}{\gamma} = \frac{1}{\alpha} + \frac{1}{\Gamma_s} + \frac{1}{\Gamma_d} \quad (2)$$

Here,  $\alpha$  is the accommodation coefficient, which in this case we assume not to be rate limiting and set as 1.  $\Gamma_d$  is related to diffusive limitation to the uptake and, in tubular geometry, is approximated by:

$$\Gamma_d = \frac{3.66(2D_g)}{\bar{c}r} \quad (3)$$

where  $r$  (cm) is the radius of the tube,  $\bar{c}$  ( $\text{cm s}^{-1}$ ) is the mean thermal velocity and  $D_g$  a diffusion coefficient ( $\text{cm}^2 \text{s}^{-1}$ ). Temperature and pressure dependent diffusion coefficients for HO, HO<sub>2</sub>, CH<sub>3</sub>O<sub>2</sub> and CH<sub>3</sub>C(O)O<sub>2</sub> were calculated from

$$D(R, \text{air}) = \frac{1.0868T^{1.75}}{\sqrt{M(R, \text{air})} \left( \sqrt[3]{V_R} + \sqrt[3]{V_{\text{air}}} \right)^2} \quad (4)$$

Where  $M$  is the reduced mass of  $R$  in air,  $R$  is one of HO, HO<sub>2</sub>, CH<sub>3</sub>O<sub>2</sub> or CH<sub>3</sub>C(O)O<sub>2</sub>, and  $V$  is the diffusion volume, which can be calculated from diffusion volumes for the individual atoms of each radical (Fuller et al., 1966).

In the case of a Langmuir–Hinshelwood reaction, we have:

$$\Gamma_s = A \frac{K_{\text{LangC}}}{(1 + K_{\text{LangC}}[R])} \quad (5)$$

A is a composite term:

$$A = \frac{4k_s[Y]N_{\max}}{\bar{c}} \quad (6)$$

where  $k_s$  is the rate constant for the accommodated trace gas with a surface site  $Y$ ,  $K_{\text{LangC}}$  and  $N_{\max}$  describe the equilibrium partitioning of  $\text{RO}_2$  to the surface.

We treat  $A$  as a variable for optimising agreement between observations and the numerical simulation. In doing this we make some broad simplifications: we take into account the temperature and molecular mass dependence of the mean thermal velocity of  $\text{HO}_2$ ,  $\text{CH}_3\text{O}_2$  and  $\text{CH}_3\text{C(O)O}_2$  but do not consider the unknown temperature dependence of terms such as  $k_s$  and  $K_{\text{LangC}}$ . We further assume that these terms have the same value for all the peroxy radicals involved and sum the concentrations of the peroxy radicals at each time step, so that  $[\text{RO}_2]$  in the above expression is equal to  $[\text{CH}_3\text{C(O)O}_2] + [\text{CH}_3\text{O}_2] + [\text{HO}_2]$ .

We derive temperature and pressure and thus time dependent values of  $\gamma$  for each peroxy radical involved. This is then converted to individual wall losses using:

$$k_{\text{wall}}(\text{RO}_2) = \frac{\gamma\bar{c}}{2r} \quad (7)$$

The time dependent values of  $k_{\text{wall}}$  varied between  $0.3$  and  $0.8\text{ s}^{-1}$  with an average value (over the transport time through the ovens and cavities) of  $\sim 0.5\text{ s}^{-1}$ , which is similar to the values of  $0.2$  and  $0.3\text{ s}^{-1}$  derived for Teflon and Quartz surface reported previously (Wooldridge et al., 2010).

The results of the simulations are shown as the solid blue lines in Figs. 7 and 8. In all cases the same reaction scheme has been applied with only the initial concentration of PAN varied to reproduce the dataset. The simulations reproduce the experimental data reasonably well over large variation in PAN ( $\sim 700$  to  $\sim 7000$  pptv) and  $\text{NO}/\text{NO}_2$ , indicating that the reaction scheme is a reasonable representation of the processes taking place. Some deviation (at  $[\text{NO}] > \sim 3$  ppb) between the measurement and model for

## TD-CRDS for $\text{NO}_2$ , $\text{RO}_2\text{NO}_2$ and $\text{RONO}_2$

J. Thieser et al.

Title Page

Abstract

Introduction

Conclusions

References

Tables

Figures

◀

▶

◀

▶

Back

Close

Full Screen / Esc

Printer-friendly Version

Interactive Discussion



the experiment with PAN = 1.05 ppbv is observed which (at 7 ppbv) amounts to ~ 25 %. This was largely due to fluctuations in the PAN source during this particular experiment and the apparent discrepancy disappears when normalised to the PAN amount as shown below for the same dataset.

5 The results of one experiment in which both PAN (~ 560 pptv) and NO (500 pptv) were initially present, and in which NO<sub>2</sub> was varied, are also captured well by the simulations, showing that multicomponent mixtures are also correctly represented (Fig. SI 3).

10 One further test was conducted using a photochemical source of PAN which converts NO to NO<sub>2</sub> and then to PAN at a yield of > 90 % (see above). This source is free of NO and NO<sub>2</sub> in significant amounts and can deliver a calibrated PAN amount if the NO mixing ratio is well characterised. The lack of NO<sub>2</sub> in this source was confirmed by observation of (no) NO<sub>2</sub> in the unheated, reference cavity. The cavity sampling from the 473K oven displayed the expected increase in NO<sub>2</sub>, whereas the cold channel showed negligible amounts. The results are displayed in Fig. SI 4 in which we plot  
15  $[\text{NO}_2]_{\text{TD}473} - [\text{NO}_2]_{\text{ref}}$  (solid squares) against that calculated from the conversion factor of NO to PAN and the degree of dilution (solid line). The results indicate that the amount of PAN detected is slightly less than calculated at the lowest mixing ratio and that the bias is enhanced at high PAN mixing ratios, consistent with the recombination of  
20 CH<sub>3</sub>C(O)O<sub>2</sub> with NO<sub>2</sub> competing with wall loss of CH<sub>3</sub>C(O)O<sub>2</sub>. The open circles are the results of a set of simulations (random amounts of PAN) using the same model as described above and initialised with NO and NO<sub>2</sub> mixing ratios of zero. The model reproduces the negligible effect of radical recombination at the lowest PAN mixing ratios and captures the dependence of the bias on PAN over a large range (factor 10) of PAN  
25 mixing ratios, further validating its applicability to systems with varying amounts of PAN, NO and NO<sub>2</sub>.

In summary, the model simulations yield correction factors for the amount of NO<sub>2</sub> formed by PAN decomposition, which depends on the mixing ratios of PAN, NO and NO<sub>2</sub>. For example, ambient mixing ratios of ~ 550 pptv PAN, ~ 520 pptv NO and

Title Page

Abstract

Introduction

Conclusions

References

Tables

Figures



Back

Close

Full Screen / Esc

Printer-friendly Version

Interactive Discussion



TD-CRDS for NO<sub>2</sub>,  
RO<sub>2</sub>NO<sub>2</sub> and RONO<sub>2</sub>

J. Thieser et al.

Title Page

Abstract

Introduction

Conclusions

References

Tables

Figures

◀

▶

◀

▶

Back

Close

Full Screen / Esc

Printer-friendly Version

Interactive Discussion



2100 pptv NO<sub>2</sub>, would result in detection of 518 pptv NO<sub>2</sub> in the TD channel, which thus has a bias of −32 pptv, requiring a correction factor of 1.06 (i.e. 6%). For similar PAN and NO<sub>2</sub> concentrations, but with NO reduced to close to zero (e.g. at night) the correction factor increases to 1.28. Correction factors less than unity are only found when NO is in excess of NO<sub>2</sub>. E.g. for 550 pptv of PAN with 5100 pptv NO and 1600 pptv NO<sub>2</sub>, the correction factor is 0.55.

In Sect. 4 we apply PAN, NO and NO<sub>2</sub>-concentration dependent correction factors to a set of data from a field campaign (PARADE, 2011). In order to do this the results of > 90 000 simulations were stored in a look-up table from which correction factors for triads of PAN-NO-NO<sub>2</sub> mixing ratios could be read. The results of the full set of simulations are summarised in Fig. SI 5. As expected, correction factors greater than unity are associated with high NO<sub>2</sub> mixing ratios and those less than unity with large NO mixing ratios. In both cases, the correction factor is smallest when PAN is low (at the limit of zero PAN, there are no RO<sub>2</sub> to recombine with or generate NO<sub>2</sub>).

**723 K inlet:**

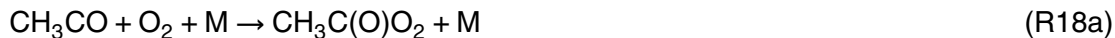
At the higher temperatures of the 723 K inlet, the chemistry of acetyl and acetyl peroxy radicals is significantly modified compared to that detailed above. The main difference is that the CH<sub>3</sub>C(O)O<sub>2</sub> radical initially formed in PAN decomposition is thermally unstable and can decompose to the acetyl radical (CH<sub>3</sub>CO) and O<sub>2</sub> (Reaction R15a) or isomerise to CH<sub>2</sub>C(O)OOH (Reaction R15b) (Lee et al., 2002; Carr et al., 2011):



The major fate of CH<sub>2</sub>C(O)OOH is thermal decomposition to OH and a singlet  $\alpha$ -lactone (Carr et al., 2011).



The acetyl radical formed in Reaction (R15a) can decompose to  $\text{CH}_3 + \text{CO}$  (Reaction R17) or react with  $\text{O}_2$  to reform the peroxy radical (Reaction R18a) or form OH (Reaction R18b) and the singlet  $\alpha$ -lactone (Groß et al., 2014; Tyndall et al., 1995; Carr et al., 2007, 2011; Chen and Lee, 2010; Papadimitriou et al., 2015):



The  $\text{CH}_3$  formed in Reaction (R17) will react with  $\text{O}_2$  to form the methylperoxy radical (Reaction R19).

At 723 K, Reactions (R15)–(R18) proceed on timescales of ms or shorter, the net effect being destruction of  $\text{CH}_3\text{C}(\text{O})\text{O}_2$  on a time scale that is short relative to its other loss processes including loss at the wall, recombination with  $\text{NO}_2$  or reaction with  $\text{NO}$ . The radical products formed in these steps are OH and  $\text{CH}_3\text{O}_2$ . The loss of  $\text{CH}_3\text{C}(\text{O})\text{O}_2$  at 723 K will obviously reduce the potential for reformation of PAN via Reaction (R10) so that the effect of adding  $\text{NO}_2$  should be significantly reduced when compared to the inlet at 473 K. The reaction of  $\text{CH}_3\text{O}_2$  with  $\text{NO}_2$  also forms a peroxyxynitrate ( $\text{CH}_3\text{O}_2\text{NO}_2$ ), but one which is unstable with respect to decomposition back to reactants even at moderate temperatures and this reaction does not lead to significant sequestering of  $\text{NO}_2$ .

The effect of adding  $\text{NO}_2$  was explored in a set of experiments with different initial PAN mixing ratios and with  $\text{NO}_2$  varied up to  $\sim 20$  ppbv. The results are displayed in Fig. 9 which plots the ratio of  $\text{NO}_2$  from PAN thermal dissociation to the amount of PAN added vs.  $[\text{NO}_2]$  added. Ideally, in the case of complete dissociation of PAN to  $\text{NO}_2$  and no subsequent recombination, this should be close to a value of unity and independent of the mixing ratio of  $\text{NO}_2$  added and this is indeed what is observed when sampling from the 723 K inlet. We conclude that, at 723 K there are insufficient peroxy radicals

TD-CRDS for  $\text{NO}_2$ ,  
 $\text{RO}_2\text{NO}_2$  and  $\text{RONO}_2$ 

J. Thieser et al.

Title Page

Abstract

Introduction

Conclusions

References

Tables

Figures

◀

▶

◀

▶

Back

Close

Full Screen / Esc

Printer-friendly Version

Interactive Discussion



TD-CRDS for NO<sub>2</sub>,  
RO<sub>2</sub>NO<sub>2</sub> and RONO<sub>2</sub>

J. Thieser et al.

Title Page

Abstract

Introduction

Conclusions

References

Tables

Figures



Back

Close

Full Screen / Esc

Printer-friendly Version

Interactive Discussion



to remove NO<sub>2</sub>, and that measurements using this inlet are insensitive to variations in ambient NO<sub>2</sub> up to about 20 ppbv. By way of comparison we also plot the data obtained using the 473 K inlet in the same manner to emphasise the significant dependence on added NO<sub>2</sub> in the cooler inlet as described above.

5 A similar set of experiments was carried out with NO added instead of NO<sub>2</sub>, in this case to investigate potential bias from oxidation of ambient NO to NO<sub>2</sub> as seen for the 473 K inlet. The results are presented in Fig. 10 which plots the ratio of NO<sub>2</sub> from PAN thermal dissociation to the amount of PAN added vs. [NO] added. In the absence of any unwanted NO<sub>2</sub> formation resulting from NO oxidation, the results should be a flat line with an intercept of 1. Figure 10 shows that NO is converted to NO<sub>2</sub> in the 723 K inlet, though the effect is much reduced when compared to the 473 K inlet. For example, the effect of adding 10 ppb NO<sub>2</sub> is to bias the PAN measured by a factor 2.75 sampling from the 473 K inlet and 1.5 when sampling from the 723 K inlet. There is no significant difference in the bias when PAN was varied between 1 and 2.5 ppb. Note that the data plotted here for the 473 K inlet is the same as that in Fig. 8.

15 As described in detail above, the large bias seen when sampling from the 473 K inlet results largely from reactions of CH<sub>3</sub>C(O)O<sub>2</sub> with NO. As CH<sub>3</sub>C(O)O<sub>2</sub> decomposes rapidly at 723 K, the oxidation of NO to NO<sub>2</sub> at this temperature is expected to be via the CH<sub>3</sub>O<sub>2</sub> radicals formed in Reactions (R17) and (R18) and also via conversion of CH<sub>3</sub>O<sub>2</sub> to HO<sub>2</sub> in the presence of NO/O<sub>2</sub> (Reaction R12). This could be qualitatively confirmed by extending the simulations described above to cover the temperatures of the 723 K inlet. In order to do this, we scaled the temperature profile to peak at 723 K (instead of at 473 K) and also added Reactions (R15)–(R19). The rate coefficients used were from Baulch et al. (2005) (Reaction R17), (Papadimitriou et al., 2015) (Reaction R18a and R18b) with the dissociation and isomerisation rate constants taken from Lee et al. (Lee et al., 2002). We note that, as these rate constants are poorly characterised at 723 K and that, even at 298 K, there is disagreement concerning e.g. the yield of OH from CH<sub>3</sub>CO + O<sub>2</sub> (Groß et al., 2014; Carr et al., 2007; Papadimitriou et al., 2015), perfect agreement between observation and simulation is not expected. The simulation shown

TD-CRDS for NO<sub>2</sub>,  
RO<sub>2</sub>NO<sub>2</sub> and RONO<sub>2</sub>

J. Thieser et al.

Title Page

Abstract

Introduction

Conclusions

References

Tables

Figures



Back

Close

Full Screen / Esc

Printer-friendly Version

Interactive Discussion



in Fig. 10 (blue line, labelled A) does however capture the observed reduction in oxidation of NO to NO<sub>2</sub> in the 723 K inlet compared to the 473 K inlet (blue line, labelled “C”). Simulation “C” was obtained using the same simulation but with the temperature profile for the 473 K inlet.

The amount of NO<sub>2</sub> formed depends on the abundance of CH<sub>3</sub>O<sub>2</sub> and HO<sub>2</sub>, so that the simulated NO<sub>2</sub> generation is favoured by higher rates of CH<sub>3</sub>C(O)O<sub>2</sub> dissociation to CH<sub>3</sub>CO rather than isomerisation to CH<sub>2</sub>C(O)OOH and higher rates of CH<sub>3</sub>CO dissociation to CH<sub>3</sub> relative to reaction with O<sub>2</sub>, which ultimately leads to OH (which can remove NO<sub>2</sub> by forming HNO<sub>3</sub>) rather than CH<sub>3</sub>O<sub>2</sub> or HO<sub>2</sub>. An improved match between observation and model (Fig. 10, blue curve marked “B”) was achieved by reducing the rate of isomerisation of CH<sub>3</sub>C(O)O<sub>2</sub> to CH<sub>2</sub>C(O)OOH to 20% of the value reported by Lee et al. (2002) at 723 K. This value is strongly dependent on calculated barrier heights and is particularly uncertain, as has been noted by Carr et al. (2011). We do not seek to imply that our data constrain this kinetic parameter as there are certainly other factors that can also affect the NO<sub>2</sub> production rate, including the rates of wall losses of radicals and the relative rates of decomposition and isomerisation of CH<sub>3</sub>C(O)O<sub>2</sub> and the thermal stability of CH<sub>3</sub>CO.

In summary, in the absence of ANs, the experiments sampling PAN via the 723 K inlet reveal that there is no significant bias when adding NO<sub>2</sub>, and that the (positive) bias introduced by the addition of NO is independent of the amount of PAN, at least up to 2–3 ppbv PAN. This simplification of the chemistry compared to the 473 K inlet removes the need for complex simulations to correct the dataset. The NO<sub>2</sub> mixing ratio resulting from the presence of PAN and NO in the 723 K inlet is adequately described by the expression  $\text{PAN} \times (1 + 0.9(1 - \exp(-0.08 \times \text{NO})))$  with NO being the NO mixing ratio in ppb (solid black line in Fig. 10), which returns correction factors of 0.94 at 1 ppb NO and ~ 0.64 at ~ 10 ppbv NO and is valid from NO mixing ratios of up to about 10 ppbv. These NO dependent factors must be applied to the PAN mixing ratios prior to subtracting them from the total NO<sub>2</sub> signal (from ΣANs + ΣPANs) when sampling from the 723 K inlet.



We now consider the chemistry taking place when ANs are present. For the 723 K inlet and considering 2-propylnitrate the additional reactions are:



The  $\text{CH}_3$  radical is immediately converted to  $\text{CH}_3\text{O}_2$  so that the radical pool is again a mixture of  $\text{CH}_3\text{O}_2$  and  $\text{HO}_2$ , both of which may convert  $\text{NO}$  to  $\text{NO}_2$ . As neither  $\text{CH}_3\text{O}_2\text{NO}_2$  nor  $\text{HO}_2\text{NO}_2$  are sufficiently thermally stable to sequester  $\text{NO}_2$  these radicals should not lead to loss of  $\text{NO}_2$  via recombination. In the 723 K inlet, this chemical system should therefore behave similarly to the one described above for PAN, i.e. should suffer from positive bias when adding  $\text{NO}$  but no negative bias when adding  $\text{NO}_2$ .

The results from a set of experiments to explore the effects of adding  $\text{NO}_2$  to various amounts of 2-propylnitrate are displayed in Fig. 11.  $\text{NO}_2$  was varied between  $\sim 0.5$  and 12 ppb for 2-propylnitrate mixing ratios of 0.35, 0.75 and 2.6 ppb. The bias from adding  $\text{NO}_2$  at these levels is not measurable at the lowest 2-propylnitrate mixing ratios, though the data at 2.6 ppb indicate a weak reduction in the measured AN mixing ratio. The model described above was extended with Reactions (R20) to (R22) and initiated with the 2-propylnitrate mixing ratios observed in the absence of extra  $\text{NO}_2$ . The results are shown by the blue lines in Fig. 11. Once again the model satisfactorily predicts the trends observed for each experiment, including the weak loss (5%) of  $\text{NO}_2$  observed at the highest 2-propylnitrate mixing ratio. The simulations revealed that the sole significant “reservoir” of this missing 5% of 2-propylnitrate was in the form of  $\text{CH}_3\text{O}_2\text{NO}_2$ .

Experiments with various amounts of added  $\text{NO}$  are summarised in Fig. 12. The positive bias caused by oxidation of  $\text{NO}$  to  $\text{NO}_2$  is apparent, and at  $\text{NO}$  mixing ratios of 8 ppb results in a  $\sim 60\%$  overestimation of the 2-propylnitrate mixing ratio. The model

Title Page

Abstract

Introduction

Conclusions

References

Tables

Figures

◀

▶

◀

▶

Back

Close

Full Screen / Esc

Printer-friendly Version

Interactive Discussion



(blue lines) also indicates that this is expected, the main oxidant of NO being CH<sub>3</sub>O<sub>2</sub>. The effect of adding 5 ppb of NO<sub>2</sub> is not observable, consistent with the weak effects described above in the absence of NO.

A more detailed look at the relative bias caused by adding NO is provided by Fig. 13, which plots the ratio of the AN signal in the presence of NO to that without added NO. There is no clear trend in the dataset with the largest effects (i.e. the uppermost and lowermost data points not associated with the extremes of 2-propylnitrate mixing ratios). The positive bias caused by the presence of NO is adequately described by the expression  $1 + 1.8(1 - \exp(-0.08 \times \text{NO}))$  with NO being the NO mixing ratio in ppb. This is plotted as the solid black line in Fig. 13. The blue lines are the model prediction when initialised with 0.56 (upper blue line) and 5.78 ppbv (lower blue line) 2-propylnitrate, respectively. The model correctly predicts the strong response of adding NO and the weak effects caused by using two different 2-propylnitrate concentrations that differ by a factor of  $\sim 10$ .

We conclude that the (negative) bias caused by addition of NO<sub>2</sub> to samples of 2-propylnitrate is small and, to a good approximation, independent of the 2-propylnitrate mixing ratio. The positive bias caused by oxidation of NO (by CH<sub>3</sub>O<sub>2</sub>) is sufficiently large to require correction, the appropriate factor given by the inverse of the expression  $1 + 1.8(1 - \exp(-0.08 \times \text{NO}))$ .

As a final test of our understanding of the chemistry, experiments were conducted in which the four components: NO (0.5 ppbv), NO<sub>2</sub> (varied) PAN (0.53 ppb) and 2-propylnitrate (0.19 ppb) were present. The results are displayed in Fig. 14. The model (blue lines) correctly predicts the total signal observed in both channels allowing us to conclude that, within experimental error, the model chemistry simulates the effects of radical recombination and radical induced oxidation of NO to NO<sub>2</sub> in both inlets/cavities.

In summary, the correction procedure when sampling from the 453 and 723 K inlets is as follows: (1) We use the model simulation results in the form of look-up-tables with measured NO and NO<sub>2</sub> concentrations and the total signal  $[\text{NO}_2]_{\text{TD473}} - [\text{NO}_2]_{\text{ref}}$  to derive (by inversion) the correct PAN mixing ratios. (2) This PAN mixing ratio is used

Title Page

Abstract

Introduction

Conclusions

References

Tables

Figures



Back

Close

Full Screen / Esc

Printer-friendly Version

Interactive Discussion



to calculate its (NO dependent) contribution to the observed total NO<sub>2</sub> measured when sampling from the 723 K inlet. This contribution is subtracted and the result divided by 1 + 1.8(1 - exp(-0.08 × NO)). This leads to the final expression to derive corrected ΣANs:

$$5 \quad [\text{ANs}] = \frac{[\text{NO}_2]_{\text{TD723}} - [\text{NO}_2]_{\text{ref}} - [\text{PAN}]F_1}{F_2} \quad (8)$$

With correction factors  $F_1 = 1 + 0.9(1 - \exp(-0.08[\text{NO}]))$  and  $F_2 = 1 + 1.8(1 - \exp(-0.08[\text{NO}]))$ , where [i] are mixing ratios in ppbv. When the NO mixing ratio is zero Eq. (8) reduces to:  $[\text{ANs}] = [\text{NO}_2]_{\text{TD723}} - [\text{NO}_2]_{\text{ref}} - [\text{PAN}]$ .

10 The laboratory tests we describe above provide insight into the radical reactions that take place in the heated inlets. The tests were conducted with PAN as a representative peroxy nitrate and with 2-propylnitrate representing alkylnitrates. Although the initial thermal decomposition of other PNs and ANs is likely to be follow a very similar pattern (Wooldridge et al., 2010; Perring et al., 2013; Day et al., 2002), we cannot rule out that the organic radicals formed with e.g. different functional groups will behave somewhat differently and would thus require modified correction factors. Comparison with 15 instruments measuring both speciated and summed PNs and ANs would be required to examine this.

### 2.1.8 Other absorbing trace gases at 405–408.5 nm

20 The potential for systematic error owing to light absorption at 405 or 408.5 nm is limited to a small number of trace gases that absorb at such wavelengths. Those known to be present in the atmosphere are dicarbonyls such as glyoxal (CH(O)CH(O)), methylglyoxal (CH<sub>3</sub>C(O)CH(O)) and biacetyl (CH<sub>3</sub>C(O)CH<sub>3</sub>C(O)) which are formed from the degradation of many volatile organic compounds including isoprene and aromatics (Atkinson, 1994; Calvert et al., 2000, 2002). The absorption cross sections of these di-carbonyls at wavelengths between 405 and 410 nm are approximately 25  $6(\pm 2) \times 10^{-20} \text{ cm}^2 \text{ molecule}^{-1}$  (Atkinson et al., 2006; IUPAC, 2015; Meller et al., 1991),

Title Page

Abstract

Introduction

Conclusions

References

Tables

Figures



Back

Close

Full Screen / Esc

Printer-friendly Version

Interactive Discussion



TD-CRDS for NO<sub>2</sub>,  
RO<sub>2</sub>NO<sub>2</sub> and RONO<sub>2</sub>

J. Thieser et al.

Title Page

Abstract

Introduction

Conclusions

References

Tables

Figures

◀

▶

◀

▶

Back

Close

Full Screen / Esc

Printer-friendly Version

Interactive Discussion



about a factor 10 lower than those of NO<sub>2</sub> (see Fig. 2). Although high mixing ratios of e.g. glyoxal (> 1 ppbv) have been observed in polluted environments (Volkamer et al., 2005a) its contribution to absorption is estimated to be insignificant compared to NO<sub>2</sub> (Fuchs et al., 2009). In rural environments peak mixing ratios of glyoxal and methylglyoxal of up to 200–300 pptv have been reported (Yin-Nan et al., 1995; Huisman et al., 2011). This would generate a bias of ~ 20–30 pptv in the NO<sub>2</sub> measurement, which corresponds to an error of five percent if NO<sub>2</sub> levels are less than ~ 400 pptv.

NO<sub>3</sub> radicals also absorb at 405 nm, with a cross-section of ~ 3 × 10<sup>-20</sup> cm<sup>2</sup> molecule<sup>-1</sup>. I.e. a factor 20 less than NO<sub>2</sub>. NO<sub>3</sub> mixing ratios of several hundred pptv (only at night) have been reported (see e.g. Crowley et al., 2010b) so that the NO<sub>3</sub> contribution to extinction at ~ 400 nm could exceed that of the di-carbonyls discussed above. However, as NO<sub>2</sub> serves as precursor to NO<sub>3</sub>, its mixing ratios are always much larger so that, even if NO<sub>3</sub> was efficiently sampled into the cavity, its contribution to absorption at 405 nm would be negligible.

### 2.1.9 Detection of N<sub>2</sub>O<sub>5</sub> (473 K) and ClNO<sub>2</sub> (723 K)

Numerous studies have reported the measurement of N<sub>2</sub>O<sub>5</sub> via thermal dissociation at temperatures between 80 and 100 °C to NO<sub>3</sub>, which may be detected by CRDS at 662 nm (see e.g. Brown and Stutz, 2012, and references therein). As the co-product of the thermal dissociation is NO<sub>2</sub>, the presence of N<sub>2</sub>O<sub>5</sub> also represents a potential interference when sampling from either of the heated inlet lines. We have used the thermal dissociation of N<sub>2</sub>O<sub>5</sub> and detection of NO<sub>2</sub> using CRDS at 405 nm to detect N<sub>2</sub>O<sub>5</sub> in this manner in laboratory investigations (Tang et al., 2012).

N<sub>2</sub>O<sub>5</sub> is not present in significant mixing ratios during the day but can represent a significant fraction of oxidized nitrogen at night-time. In the dataset obtained at the PARADE campaign, we observed occasional increases in NO<sub>2</sub> when sampling from the heated inlets that were strongly correlated with the presence of N<sub>2</sub>O<sub>5</sub> (measured by TD-CRDS at 662 nm, Crowley et al., 2010b). Correction for an N<sub>2</sub>O<sub>5</sub> contribution could however not be accurately applied as the sampling efficiency (through ~ 10 m

TD-CRDS for NO<sub>2</sub>,  
RO<sub>2</sub>NO<sub>2</sub> and RONO<sub>2</sub>

J. Thieser et al.

Title Page

Abstract

Introduction

Conclusions

References

Tables

Figures



Back

Close

Full Screen / Esc

Printer-friendly Version

Interactive Discussion



of PFA tubing) was unknown but evidently less than unity as the features observed in the NO<sub>2</sub> instrument were weaker than those in the N<sub>2</sub>O<sub>5</sub> instrument. In addition, the NO<sub>3</sub> formed may also react with any NO available (generating two more NO<sub>2</sub>) or with hydrocarbons, so that the stoichiometry of N<sub>2</sub>O<sub>5</sub> to NO<sub>2</sub> conversion may be variable.

For the PARADE campaign dataset we therefore chose to eliminate data during episodes of high N<sub>2</sub>O<sub>5</sub> (> 150 pptv). We conclude that undesired detection of N<sub>2</sub>O<sub>5</sub> as NO<sub>2</sub> when sampling from the heated inlets can be a significant source of uncertainty when measuring ΣPN at night-time, especially if measurements of N<sub>2</sub>O<sub>5</sub> are not available. As both heated channels will decompose N<sub>2</sub>O<sub>5</sub> to NO<sub>2</sub> the ΣANs measurement (obtained as the difference signal) should not be impacted by the presence of N<sub>2</sub>O<sub>5</sub>.

A potential interference specific to the 723 K channel results from the thermal decomposition of ClNO<sub>2</sub>, which is formed in the heterogeneous reaction of N<sub>2</sub>O<sub>5</sub> on chloride containing particles at night-time. In a series of laboratory experiments using this instrument (Fig. SI 6) we showed that a sample of ClNO<sub>2</sub> was detected as NO<sub>2</sub> at oven temperatures above ~ 680 K, consistent with that reported by Thaler et al. (2011). As ClNO<sub>2</sub> can represent a significant fraction of NO<sub>2</sub> at night-time and in the early morning (see e.g. Osthoff et al., 2008; Phillips et al., 2012; Wagner et al., 2012; Mielke et al., 2013; Thornton et al., 2010) it will represent a significant source of uncertainty in ΣANs measurements when present. In this case, the only correction possibility requires the simultaneous measurement of ClNO<sub>2</sub>. During the PARADE campaign (see later) early morning ClNO<sub>2</sub> levels approached 800 pptv so that large corrections had to be applied to extract ΣANs during these periods.

### 2.1.10 Precision

The precision of the measurements of NO<sub>2</sub> in the reference cavity and TD-cavities was derived by continuous sampling of zero air. Equivalent NO<sub>2</sub> mixing ratios were calculated for conditions of 670 Torr and 35 °C. The results are summarised in Fig. 15 where the upper panel shows the raw data converted to NO<sub>2</sub> mixing ratio-equivalents. The

TD-CRDS for NO<sub>2</sub>,  
RO<sub>2</sub>NO<sub>2</sub> and RONO<sub>2</sub>

J. Thieser et al.

Title Page

Abstract

Introduction

Conclusions

References

Tables

Figures

◀

▶

◀

▶

Back

Close

Full Screen / Esc

Printer-friendly Version

Interactive Discussion



regular spaces in the data are zeroing periods as they would have been measured in a normal experiment. The baseline which is plotted for a two hour time interval here shows no long term trend, indicating that the zero measurements every 5–10 min are sufficient to capture drifts in ring-down related to the variability of the cavity performance. The lower panel is an Allan deviation plot for this cavity (red curve), which shows that the 1  $\sigma$  precision increases for integration times up to  $\sim 40$  s and follows the expected square root dependence (red, dashed line) up to an integration time of  $\sim 10$  s. The precision at 1 s integration time is 28 pptv, improving to 5–6 pptv at 40 s.

The precision obtained with the TD-cavity (sampling from the 723 K inlet) was investigated by adding a constant mixing ratio ( $\sim 700$  pptv) of *i*-propylnitrate and measuring the difference signal between the reference and TD-cavities. These results are shown in the middle panel (raw data) and in the Allan deviation plot (blue lines). The precision of the measurement improves from  $\sim 10\%$  for 4 s integration time to about 3% for 1 min integration time and follows a square root dependence up to  $\sim 10$  s integration time.

### 2.1.11 Total uncertainty

#### NO<sub>2</sub> measurement

Several sources of systematic error may contribute to the total uncertainty of the NO<sub>2</sub> measurements in the reference cavity; these are:

- Error in determination of the effective cross section  $\sigma_{\text{Laser}}: \leq 5\%$ , which also accounts for uncertainty in the absolute NO<sub>2</sub> cross sections of Voigt et al. (2002).
- Wavelength stability of the laser emission over longer measurement periods:  $\leq 3\%$  based on variability of the emission spectra (recorded at 20 min intervals).
- Error in  $l/d$  ratio:  $\sim 1\%$  (see above)
- Error in pressure and temperature stability of the cavities:  $\sim 0.5\%$
- NO<sub>2</sub> mixing ratio in zero air bottles:  $< 20$  pptv (see above)

– Error in humidity correction: considering the difference in values of  $\Delta\sigma_{\text{Rayleigh}}^{405-409\text{ nm}}$  derived in this work and those of Fuchs et al. (2009) (see Sect. 2.1.3) we estimate an error of about 20 % in this correction factor. This converts to an error of  $\leq 20$  pptv at 100 % RH.

– Possible interference from other absorbers: normally negligible but must be assessed on a case-to-case basis.

At very low NO<sub>2</sub> mixing ratios the uncertainty of the NO<sub>2</sub> measurements is therefore mainly influenced by the amount of NO<sub>2</sub> within the zero air bottles and the correction applied for the scattering effect of ambient H<sub>2</sub>O, whilst at larger NO<sub>2</sub> mixing ratios the uncertainty is mainly determined by the uncertainty in the effective cross section and laser stability. The uncertainty of the NO<sub>2</sub> measurement stemming from systematic errors is thus 6 % + 20 pptv + (20 pptv \* RH/100), where RH is in percent. For any given integration period, the total uncertainty may be obtained by adding the precision quoted above and is e.g. 11 % + 30 pptv for 40 s sampling period with a relative humidity of 50 %.

### $\Sigma$ PNs measurement

As this is a difference measurement, the uncertainty in the corrections for the potential presence of NO<sub>2</sub> in the zero air or errors in  $\Delta\sigma_{\text{Rayleigh}}^{405-409\text{ nm}}$  do not contribute to overall uncertainty. The major source of uncertainty is associated with the corrections made for reactions of radical fragments with NO and NO<sub>2</sub> (Sect. 2.1.7). Although performing the correction via modelling of the chemistry in the hot inlets and subsequent tubing is clearly complex, the fact that laboratory data covering a large parameter space can be simulated well indicates that the error in the correction is less than 15 % at the largest PAN, NO and NO<sub>2</sub> mixing ratios investigated. However, as we have only performed these tests for PAN and not for other peroxy acyl nitric anhydrides, we increase the maximum uncertainty on this correction factor to 30 %. As the size of the correction

[Title Page](#)
[Abstract](#)
[Introduction](#)
[Conclusions](#)
[References](#)
[Tables](#)
[Figures](#)
[Back](#)
[Close](#)
[Full Screen / Esc](#)
[Printer-friendly Version](#)
[Interactive Discussion](#)


[Title Page](#)[Abstract](#)[Introduction](#)[Conclusions](#)[References](#)[Tables](#)[Figures](#)[Back](#)[Close](#)[Full Screen / Esc](#)[Printer-friendly Version](#)[Interactive Discussion](#)

increases non-linearly with each of PAN NO and NO<sub>2</sub> mixing ratios no single uncertainty can be given. As an example, at 1 ppb PAN, the correction factor required in the presence of 1 ppb NO and 5 ppb NO<sub>2</sub> is  $1.09 \pm 0.22$ . In the absence of NO (e.g. at night-time) the same concentrations of PAN and NO<sub>2</sub> require a correction factor of  $1.52 \pm 0.30$ .

## Σ ANs measurement

As the instrument has only two measurement cavities sampling from three inlets the derivation of ΣANs while sampling from the 723 K inlet requires interpolation of the measurements from the 473 K inlet. The overall uncertainty for the ΣANs measurements thus depends on the variability of the ΣPNs measurements. A further source of uncertainty is associated with the corrections made for reactions of radical fragments with NO and NO<sub>2</sub> as described in Sect. 2.1.7. Largest errors in ΣANs will be associated with air masses with high ΣPN and low ΣANs, as this will amplify any error in the correction related to the different efficiency of sampling of ΣANs from both inlets, which itself is a function of the NO and NO<sub>2</sub> concentrations. For example, using expression E8, and adding a [NO<sub>x</sub>] dependent error to the PAN, F<sub>1</sub> and F<sub>2</sub> correction factors (increasing from 0 to 10% error when going from 0 to 5 ppb NO) we calculate a total possible error of ~ 16% if [NO<sub>x</sub>] = [PAN] = 1 ppb, increasing to ~ 50% at 5 ppb of NO.

Clearly, the accuracy of the PAN measurement and its correction will critically impact on the accuracy of the AN measurement. As we indicate later, reliable AN measurements can only be made under certain conditions.

## 3 Ambient datasets for NO<sub>2</sub>, ΣPNs and ΣANs

A summer field campaign of ~ 3 weeks duration at the Taunus Observatorium on the Kleiner Feldberg, (Crowley et al., 2010b; Phillips et al., 2012) provided opportunity for comparison of the present CRDS system for measurement of NO<sub>2</sub> and ΣPNs with



TD-CRDS for NO<sub>2</sub>,  
RO<sub>2</sub>NO<sub>2</sub> and RONO<sub>2</sub>

J. Thieser et al.

Title Page

Abstract

Introduction

Conclusions

References

Tables

Figures

◀

▶

◀

▶

Back

Close

Full Screen / Esc

Printer-friendly Version

Interactive Discussion



established instruments under variable conditions. The Taunus Observatorium is in a rural area impacted by emissions from several local cities between 30 and 40 km distant. Typical NO<sub>x</sub> levels are between 1 and 2 ppb with occasional excursions up to peak values of > 10 ppb (Crowley et al., 2010b). Summertime PAN levels of at the site had been reported as part of a PhD thesis with, campaign averaged, mid-afternoon maximum concentrations of about 1 ppb (Handisides, 2001).

### 3.1 NO<sub>2</sub> measurements

The established instruments used for comparison were (for NO<sub>2</sub>) a chemiluminescence detector (CLD) with blue-light converter and a long-path differential optical absorption spectrometer, DOAS. These instruments are described in detail elsewhere (Crowley et al., 2010b; Merten et al., 2011; Pöhler et al., 2010; Hosaynali Beygi et al., 2011; Suitters, 2012).

### TD-CRDS vs. CLD

Both instruments sampled air via PFA tubing with co-located inlets about 8 m a.g.l. and 2 m above the platform structure to which the inlets were attached. In both cases, bypass flows were used to reduce the residence time in the inlets. The TD-CRDS sampled at a rate of ~ 0.2 Hz, the CLD at ~ 1 Hz. The accuracy of the CLD measurements, defined partially by calibration accuracy, blue-light converter efficiency, and assumptions about levels of NO<sub>2</sub> in zero air, is reported to be ~ 10 % during the PARADE campaign (Li et al., 2015).

The data displayed in Fig. 16 (left panel) shows the correlation between 1 min averaged NO<sub>2</sub> mixing ratios derived by these two instruments. The error bars are the reported standard deviation over the sampling interval, and reflect atmospheric variability rather than instrument precision. Agreement is good with a slope  $0.906 \pm 0.0003$  for the bivariate (York) fit to the data and an intercept of  $-115 \pm 0.7$  pptv. An unweighted fit gives values of  $0.889 \pm 0.0006$  and  $-86 \pm 2$  pptv. Irrespective of the method of weight-

ing used, the deviation of the slope from unity lies within the combined uncertainty of the instruments. A statistically significant, negative intercept as observed would be e.g. the result of low levels ( $\sim 100$  pptv) of  $\text{NO}_2$  present in the zero air used to zero the CLD, or the photochemical/surface activated decomposition (to  $\text{NO}_2$ ) of surface adsorbed trace gases (e.g. nitrates) in the blue-light converter during zeroing.

## CRDS vs. DOAS

The right-hand panel of Fig. 16 shows the correlation between the CRDS and DOAS instruments. The DOAS measured  $\text{NO}_2$  over an optical path length of  $\approx 3$  km, with the light source and spectrograph located within a few metres of the CRDS inlet. The DOAS measurements of  $\text{NO}_2$  were made every 10 min. Spatial inhomogeneity in  $\text{NO}_2$  mixing ratios will result in reduced agreement between a point measurement (CRDS) and that of the DOAS, which integrates over a large area. For this reason we compare only data in which the temporal variability in the CRDS signal results in standard deviations over the 10 min averaging interval of less than 5%. Such datasets are likely to be characterised by good spatial homogeneity over the same time period and are more suitable for comparison. The resulting slope and intercept from the weighted, bivariate fit are  $1.008 \pm 0.002$  and  $-0.034 \pm 0.006$  ppbv, respectively. The unweighted fit resulted in values of  $0.962 \pm 0.006$  and  $0.025 \pm 0.002$  ppbv, respectively, both fits indicating excellent agreement between these instruments.

We conclude that the CRDS measurements of  $\text{NO}_2$  compare well to two established instruments, confirming the experimental concept and the accuracy of the correction factors applied.

## 4 $\Sigma$ PNs measurement and comparison with PAN measured by TD-CIMS

During PARADE, speciated PANs were measured using a TD-CIMS (Phillips et al., 2013). The CIMS instrument is able to distinguish between different acyl peroxy nitrates

## TD-CRDS for $\text{NO}_2$ , $\text{RO}_2\text{NO}_2$ and $\text{RONO}_2$

J. Thieser et al.

Title Page

Abstract

Introduction

Conclusions

References

Tables

Figures

◀

▶

◀

▶

Back

Close

Full Screen / Esc

Printer-friendly Version

Interactive Discussion



TD-CRDS for NO<sub>2</sub>,  
RO<sub>2</sub>NO<sub>2</sub> and RONO<sub>2</sub>

J. Thieser et al.

Title Page

Abstract

Introduction

Conclusions

References

Tables

Figures

◀

▶

◀

▶

Back

Close

Full Screen / Esc

Printer-friendly Version

Interactive Discussion



such as PAN, PPN, MPN, while the TD-CRDS measures the sum of all the individual nitrates. The TD-CIMS requires an in-situ calibration using a photochemical source of PAN. This PAN calibration source was characterized using the TD-CRDS instrument, employing the correction factors described above. As the calibration was conducted at ~ 500 pptv of PAN, and in the absence of extra NO<sub>2</sub> or NO, the correction factor for the CRDS measurements (1.06) was small.

Figure 17 shows the comparison between the PAN measurements by CIMS and ΣPNs measured by the TD-CRDS. The correlation between the measurements is very good ( $R^2 = 0.93$ ) with a slope of 1.31 and an intercept of -34 pptv. The data are coloured according to [NO] and indicate no obvious bias due e.g. to the existence of high NO levels. The correction factors applied to the TD-CRDS dataset were in the range 0.8 and 1.5, mostly however close to  $1.15 \pm 0.1$ . This is illustrated in the frequency distribution plot in Fig. SI 7.

The slope of greater than unity indicates the presence of peroxy nitrate species such as PPN, MPAN and APAN which thus represent ~ 24 % (31/131) of total PNs. The PAN and ΣPNs measurements will be discussed in detail in a publication describing the results of the PARADE campaign. Here we simply note that the results are consistent with previous observations, which indicate that PAN is the most abundant PN in the atmosphere and usually contributes 70–90 % of the total peroxy nitrates (Roberts, 1990).

## 5 ANs measurements

A 5 day period of measurements of ΣANs with NO<sub>2</sub>, NO and ΣPNs during PARADE is shown in Fig. 18. The black data points in the ΣPNs plot (lower panel) are the raw data, the red data points have been corrected for the effects of NO and NO<sub>2</sub> as derived above. The black data points in the ΣANs plot (middle panel) are the total NO<sub>2</sub> signal when sampling from the 723 K inlet minus the NO<sub>2</sub> measured in the reference cavity and thus represent the uncorrected sum of ΣANs + ΣPNs. The red data points were

TD-CRDS for NO<sub>2</sub>,  
RO<sub>2</sub>NO<sub>2</sub> and RONO<sub>2</sub>

J. Thieser et al.

Title Page

Abstract

Introduction

Conclusions

References

Tables

Figures

◀

▶

◀

▶

Back

Close

Full Screen / Esc

Printer-friendly Version

Interactive Discussion



obtained by applying the full corrections as described. To illustrate the magnitude of the corrections, this may be compared to the green data points which were obtained simply by subtracting the NO<sub>2</sub> mixing ratios measured when sampling from the 473 K inlet from that when sampling from the 723 K inlet. The difference between the green (uncorrected) and red (corrected) datasets is mainly less than ~ 20 % but is much larger during episodes of high NO and NO<sub>2</sub> e.g. at day 236.8 (upper panel). During this period, the ANs values are partially negative, which may indicate a bias in the correction factor at high NO<sub>x</sub>. For a particular set of conditions, reliable data (i.e. small correction factors) were obtained for NO<sub>x</sub> < 5 ppb. As noted above, a more detailed analysis of this and the ΣPNs data set will be presented elsewhere.

## 6 Conclusions and outlook

We have developed, tested and deployed a two-cavity (405.2 and 408.5 nm) instrument with three different inlets for the measurement of ambient NO<sub>2</sub>, ΣPN and ΣAN. NO<sub>2</sub> is measured directly with a total uncertainty of 6 % + 20 pptv + (20 pptv × RH/100), where RH is in percent. PNs and ANs are detected via thermal dissociation to NO<sub>2</sub> and extensive laboratory characterisation of the instrument, including numerical simulation of the radical chemistry in both heated inlets, was carried out in order to derive correction factors that account for bias caused by the competing effects of radical recombination and oxidation of ambient NO. The requirement to correct the ΣAN and ΣPN datasets limits the application of this prototype instrument to regions of low-to moderate NO<sub>x</sub> levels (< 5 ppb).

The first field deployment (PARADE) showed favourable comparison with other NO<sub>2</sub> and ΣPN measurements (chemiluminescence detector with blue-light-converter and long-path differential optical absorption spectroscopy for NO<sub>2</sub>, and chemical ionisation mass spectrometry for ΣPNs). During the campaign, the correction factor for PNs was, on average between 0.8 and 1.2, depending on the relative NO and NO<sub>2</sub> concentrations.

TD-CRDS for NO<sub>2</sub>,  
RO<sub>2</sub>NO<sub>2</sub> and RONO<sub>2</sub>

J. Thieser et al.

Title Page

Abstract

Introduction

Conclusions

References

Tables

Figures



Back

Close

Full Screen / Esc

Printer-friendly Version

Interactive Discussion



Future improvements will involve the use of humidified, zero-air to reduce uncertainty resulting from optical scattering of atmospheric water vapour, which will improve the accuracy of the data at low NO<sub>x</sub> levels. We shall also explore other signal acquisition hardware/software options with the goal of increasing the sampling rate and improving the detection limit for all channels.

Most importantly, we shall investigate means of reduction of the impact of organic radical reactions in the hot inlets by heterogeneous scavenging of e.g. CH<sub>3</sub>C(O)O<sub>2</sub> and other RO<sub>x</sub> species and also by reduction of the pressure and gas residence time in the inlets and cavities. These measures will reduce the total uncertainty in the PN<sub>s</sub> and AN<sub>s</sub> measurements and extend the operational range of the instrument to higher NO<sub>x</sub> regimes.

**The Supplement related to this article is available online at doi:10.5194/amtd-8-11533-2015-supplement.**

*Acknowledgements.* This work was carried out in part fulfilment of the PhD of J. Thieser, who thanks U. Platt for many helpful discussions and supervision of his thesis. We thank Christoph Groß for assistance in preparing the PAN sample. We thank Simone Stöppler and Thomas Elsinger of the “Hessischer Rundfunk” for mounting the DOAS retro-reflectors on the tower at the Großer Feldberg. We are grateful to Dupont for providing a sample of the FEP suspension used to coat the inlets and cavities.

The article processing charges for this open-access publication were covered by the Max Planck Society.

## References

- Atherton, C. S. and Penner, J. E.: The transformation of nitrogen oxides in the polluted troposphere, *Tellus B*, 40, 380–392, 1988.
- Atkinson, R.: Gas-phase tropospheric chemistry of organic compounds, *J. Phys. Chem. Ref. Data*, monograph Nr. 2, 1–216, 1994.
- Atkinson, R. and Arey, J.: Atmospheric degradation of volatile organic compounds, *Chem. Rev.*, 103, 4605–4638, doi:10.1021/cr0206420, 2003.
- Atkinson, R., Baulch, D. L., Cox, R. A., Crowley, J. N., Hampson, R. F., Hynes, R. G., Jenkin, M. E., Rossi, M. J., and Troe, J.: Evaluated kinetic and photochemical data for atmospheric chemistry: Volume I - gas phase reactions of O<sub>x</sub>, HO<sub>x</sub>, NO<sub>x</sub> and SO<sub>x</sub> species, *Atmos. Chem. Phys.*, 4, 1461–1738, doi:10.5194/acp-4-1461-2004, 2004.
- Atkinson, R., Baulch, D. L., Cox, R. A., Crowley, J. N., Hampson, R. F., Hynes, R. G., Jenkin, M. E., Rossi, M. J., Troe, J., and IUPAC Subcommittee: Evaluated kinetic and photochemical data for atmospheric chemistry: Volume II – gas phase reactions of organic species, *Atmos. Chem. Phys.*, 6, 3625–4055, doi:10.5194/acp-6-3625-2006, 2006.
- Atlas, E.: Evidence for > C<sub>3</sub> alkyl nitrates in rural and remote atmosphere, *Nature*, 331, 426–428, 1988.
- Ayers, J. D., Apodaca, R. L., Simpson, W. R., and Baer, D. S.: Off-axis cavity ringdown spectroscopy: application to atmospheric nitrate radical detection, *Appl. Optics*, 44, 7239–7242, 2005.
- Baulch, D. L., Bowman, C. T., Cobos, C. J., Cox, R. A., Just, T., Kerr, J. A., Pilling, M. J., Stocker, D., Troe, J., Tsang, W., Walker, R. W., and Warnatz, J.: Evaluated kinetic data for combustion modeling: supplement II, *J. Phys. Chem. Ref. Data*, 34, 757–1397, 2005.
- Berden, G., Peeters, R., and Meijer, G.: Cavity ring-down spectroscopy: experimental schemes and applications, *Int. Rev. Phys. Chem.*, 19, 565–607, 2000.
- Brown, S. S.: Absorption spectroscopy in high-finesse cavities for atmospheric studies, *Chem. Rev.*, 103, 5219–5238, 2003.
- Brown, S. S. and Stutz, J.: Nighttime radical observations and chemistry, *Chem. Soc. Rev.*, 41, 6405–6447, 2012.
- Browne, E. C., Perring, A. E., Wooldridge, P. J., Apel, E., Hall, S. R., Huey, L. G., Mao, J., Spencer, K. M., Clair, J. M. St., Weinheimer, A. J., Wisthaler, A., and Cohen, R. C.: Global

Title Page

Abstract

Introduction

Conclusions

References

Tables

Figures



Back

Close

Full Screen / Esc

Printer-friendly Version

Interactive Discussion



TD-CRDS for NO<sub>2</sub>,  
RO<sub>2</sub>NO<sub>2</sub> and RONO<sub>2</sub>

J. Thieser et al.

Title Page

Abstract

Introduction

Conclusions

References

Tables

Figures



Back

Close

Full Screen / Esc

Printer-friendly Version

Interactive Discussion



- and regional effects of the photochemistry of CH<sub>3</sub>O<sub>2</sub>NO<sub>2</sub>: evidence from ARCTAS, *Atmos. Chem. Phys.*, 11, 4209–4219, doi:10.5194/acp-11-4209-2011, 2011.
- Buhr, M. P., Parrish, D. D., Norton, R. B., Fehsenfeld, F. C., Sievers, R. E., and Roberts, J. M.: Contribution of organic nitrates to the total reactive nitrogen budget at a rural eastern U.S. site, *J. Geophys. Res.*, 95, 9809–9816, 1990.
- Calvert, J. G. and Madronich, S.: Theoretical-study of the initial products of the atmospheric oxidation of hydrocarbons, *J. Geophys. Res.-Atmos.*, 92, 2211–2220, 1987.
- Calvert, J. G., Atkinson, R., Kerr, J. A., Madronich, S., Moortgat, G. K., Wallington, T. J., and Yarwood, G.: *The Mechanisms of Atmospheric Oxidation of the Alkenes*, Oxford Univ. Press, New York, 2000.
- Calvert, J. G., Atkinson, R., Becker, K. H., Seinfeld, J. H., Wallington, T. J., and Yarwood, G.: *The Mechanism of Atmospheric Oxidation of Aromatic Hydrocarbons*, Oxford University Press, New York, 2002.
- Carr, S. A., Baeza-Romero, M. T., Blitz, M. A., Pilling, M. J., Heard, D. E., and Seakins, P. W.: OH yields from the CH<sub>3</sub>CO + O<sub>2</sub> reaction using an internal standard, *Chem. Phys. Lett.*, 445, 108–112, 2007.
- Carr, S. A., Glowacki, D. R., Liang, C.-H., Baeza-Romero, M. T., Blitz, M. A., Pilling, M. J., and Seakins, P. W.: Experimental and modeling studies of the pressure and temperature dependences of the kinetics and the OH yields in the acetyl + O<sub>2</sub> reaction, *J. Phys. Chem. A*, 115, 1069, 1069–1085, 2011.
- Chen, S.-Y. and Lee, Y.-P.: Transient infrared absorption of t-CH<sub>3</sub>C(O)OO, c-CH<sub>3</sub>C(O)OO, and α-lactone recorded in gaseous reactions of CH<sub>3</sub>CO and O<sub>2</sub>, *J. Chem. Phys.*, 132, 114303, doi:10.1063/1.3352315, 2010.
- Crowley, J. N., Ammann, M., Cox, R. A., Hynes, R. G., Jenkin, M. E., Mellouki, A., Rossi, M. J., Troe, J., and Wallington, T. J.: Evaluated kinetic and photochemical data for atmospheric chemistry: Volume V – heterogeneous reactions on solid substrates, *Atmos. Chem. Phys.*, 10, 9059–9223, doi:10.5194/acp-10-9059-2010, 2010a.
- Crowley, J. N., Schuster, G., Pouvesle, N., Parchatka, U., Fischer, H., Bonn, B., Bingemer, H., and Lelieveld, J.: Nocturnal nitrogen oxides at a rural mountain-site in south-western Germany, *Atmos. Chem. Phys.*, 10, 2795–2812, doi:10.5194/acp-10-2795-2010, 2010b.
- Day, D. A., Wooldridge, P. J., Dillon, M. B., Thornton, J. A., and Cohen, R. C.: A thermal dissociation laser-induced fluorescence instrument for in situ detection of NO<sub>2</sub>, peroxy nitrates, alkyl nitrates, and HNO<sub>3</sub>, *J. Geophys. Res.*, 107, 4046, doi:10.1029/2001jd000779, 2002.

TD-CRDS for NO<sub>2</sub>,  
RO<sub>2</sub>NO<sub>2</sub> and RONO<sub>2</sub>

J. Thieser et al.

Title Page

Abstract

Introduction

Conclusions

References

Tables

Figures



Back

Close

Full Screen / Esc

Printer-friendly Version

Interactive Discussion



- Day, D. A., Dillon, M. B., Wooldridge, P. J., Thornton, J. A., Rosen, R. S., Wood, E. C., and Cohen, R. C.: On alkyl nitrates, O<sub>3</sub>, and the “missing NO<sub>y</sub>”, *J. Geophys. Res.-Atmos.*, 108, 4501, doi:10.1029/2003jd003685, 2003.
- 5 Fahey, D. W., Hübler, G., Parrish, D. D., Williams, E. J., Norton, R. B., Ridley, B. A., Singh, H. B., Liu, S. C., and Fehsenfeld, F. C.: Reactive nitrogen species in the troposphere: measurements of NO, NO<sub>2</sub>, HNO<sub>3</sub>, particulate nitrate, peroxyacetyl nitrate (PAN), O<sub>3</sub>, and total reactive odd nitrogen (NO<sub>y</sub>) at Niwot Ridge, Colorado, *J. Geophys. Res.*, 91, 9781–9793, 1986.
- 10 Flocke, F. M., Weinheimer, A. J., Swanson, A. L., Roberts, J. M., Schmitt, R., and Shertz, S.: On the measurement of PANs by gas chromatography and electron capture detection, *J. Atmos. Chem.*, 52, 19–43, 2005.
- Fuchs, H., Dube, W. P., Lerner, B. M., Wagner, N. L., Williams, E. J., and Brown, S. S.: A sensitive and versatile detector for atmospheric NO<sub>2</sub> and NO<sub>x</sub> based on blue diode laser cavity ring-down spectroscopy, *Environ. Sci. Technol.*, 43, 7831–7836, doi:10.1021/es902067h, 2009.
- 15 Fuller, E. N., Schettle, P. D., and Giddings, J. C.: A new method for prediction of binary gas-phase diffusion coefficients, *Ind. Eng. Chem.*, 58, 19–27, 1966.
- Groß, C. B. M., Dillon, T. J., and Crowley, J. N.: Pressure dependent OH yields in the reactions of CH<sub>3</sub>CO and HOCH<sub>2</sub>CO with O<sub>2</sub>, *Phys. Chem. Chem. Phys.*, 16, 10990–10998, doi:10.1039/c4cp01108b, 2014.
- 20 Handisides, G. M.: The Influence of Peroxy Radicals on Ozone Production, Fachbereich Geowissenschaften, Johann Wolfgang Goethe Universität, Frankfurt am Main, 2001.
- Hao, C. S., Shepson, P. B., Drummond, J. W., and Muthuramu, K.: Gas-chromatographic detector for selective and sensitive detection of atmospheric organic nitrates, *Anal. Chem.*, 66, 3737–3743, 1994.
- 25 Hargrove, J. and Zhang, J.: Measurements of NO<sub>x</sub>, acyl peroxy nitrates, and NO<sub>y</sub> with automatic interference corrections using a NO<sub>2</sub> analyzer and gas phase titration, *Rev. Sci. Instrum.*, 79, 046109, doi:10.1063/1.2908432, 2008.
- Hosaynali Beygi, Z., Fischer, H., Harder, H. D., Martinez, M., Sander, R., Williams, J., Brookes, D. M., Monks, P. S., and Lelieveld, J.: Oxidation photochemistry in the Southern Atlantic boundary layer: unexpected deviations of photochemical steady state, *Atmos. Chem. Phys.*, 11, 8497–8513, doi:10.5194/acp-11-8497-2011, 2011.
- 30 Huisman, A. J., Hottle, J. R., Galloway, M. M., DiGangi, J. P., Coens, K. L., Choi, W., Faloon, I. C., Gilman, J. B., Kuster, W. C., de Gouw, J., Bouvier-Brown, N. C., Gold-



TD-CRDS for NO<sub>2</sub>,  
RO<sub>2</sub>NO<sub>2</sub> and RONO<sub>2</sub>

J. Thieser et al.

Title Page

Abstract

Introduction

Conclusions

References

Tables

Figures



Back

Close

Full Screen / Esc

Printer-friendly Version

Interactive Discussion



- stein, A. H., LaFranchi, B. W., Cohen, R. C., Wolfe, G. M., Thornton, J. A., Docherty, K. S., Farmer, D. K., Cubison, M. J., Jimenez, J. L., Mao, J., Brune, W. H., and Keutsch, F. N.: Photochemical modeling of glyoxal at a rural site: observations and analysis from BEARPEX 2007, *Atmos. Chem. Phys.*, 11, 8883–8897, doi:10.5194/acp-11-8883-2011, 2011.
- 5 IUPAC: Task Group on Atmospheric Chemical Kinetic Data Evaluation, Ammann, M., Cox, R. A., Crowley, J. N., Jenkin, M. E., Mellouki, A., Rossi, M. J., Troe, J., and Wallington, T. J., available at: <http://iupac.pole-ether.fr/index.html>, August 2015.
- Kley, D. and McFarland, M.: Chemiluminescence detector for NO and NO<sub>2</sub>, *Atmos. Technol.*, 12, 63–69, 1980.
- 10 LaFranchi, B. W., Wolfe, G. M., Thornton, J. A., Harrold, S. A., Browne, E. C., Min, K. E., Wooldridge, P. J., Gilman, J. B., Kuster, W. C., Goldan, P. D., de Gouw, J. A., McKay, M., Goldstein, A. H., Ren, X., Mao, J., and Cohen, R. C.: Closing the peroxy acetyl nitrate budget: observations of acyl peroxy nitrates (PAN, PPN, and MPAN) during BEARPEX 2007, *Atmos. Chem. Phys.*, 9, 7623–7641, doi:10.5194/acp-9-7623-2009, 2009.
- 15 Lee, J., Chen, C.-J., and Bozzelli, J. W.: Thermochemical and kinetic analysis of the acetyl radical (CH<sub>3</sub>CO) + O<sub>2</sub> Reaction System, *J. Phys. Chem. A*, 106, 7155–7170, doi:10.1021/jp014443g, 2002.
- Lee, L., Wooldridge, P. J., Gilman, J. B., Warneke, C., de Gouw, J., and Cohen, R. C.: Low temperatures enhance organic nitrate formation: evidence from observations in the 2012  
20 Uintah Basin Winter Ozone Study, *Atmos. Chem. Phys.*, 14, 12441–12454, doi:10.5194/acp-14-12441-2014, 2014.
- Li, J., Reiffs, A., Parchatka, U., and Fischer, H.: In situ measurements of atmospheric CO and its correlation with NO<sub>x</sub> and O<sub>3</sub> at a rural mountain site, *Metrol. Meas. Syst.*, XXII, 25–38, 2015.
- 25 Meller, R., Raber, W., Crowley, J. N., Jenkin, M. E., and Moortgat, G. K.: The UV-visible absorption spectrum of methylglyoxal, *J. Photoch. Photobio. A*, 62, 163–171, 1991.
- Merten, A., Tschirter, J., and Platt, U.: Design of differential optical absorption spectroscopy long-path telescopes based on fiber optics, *Appl. Optics*, 50, 738–754, 2011.
- Mielke, L. H. and Osthoff, H. D.: On quantitative measurements of peroxy-carboxylic nitric an-  
30 hydride mixing ratios by thermal dissociation chemical ionization mass spectrometry, *Int. J. Mass Spectrom.*, 310, 1–9, doi:10.1016/j.ijms.2011.10.005, 2012.
- Mielke, L. H., Stutz, J., Tsai, C., Hurlock, S. C., Roberts, J. M., Veres, P. R., Froyd, K. D., Hayes, P. L., Cubison, M. J., Jimenez, J. L., Washenfelder, R. A., Young, C. J., Gilman, J. B.,

TD-CRDS for NO<sub>2</sub>,  
RO<sub>2</sub>NO<sub>2</sub> and RONO<sub>2</sub>

J. Thieser et al.

Title Page

Abstract

Introduction

Conclusions

References

Tables

Figures



Back

Close

Full Screen / Esc

Printer-friendly Version

Interactive Discussion



de Gouw, J. A., Flynn, J. H., Grossberg, N., Lefer, B. L., Liu, J., Weber, R. J., and Osthoff, H. D.: Heterogeneous formation of nitryl chloride and its role as a nocturnal NO<sub>x</sub> reservoir species during CalNex-LA 2010, *J. Geophys. Res.-Atmos.*, 118, 10638–10652, doi:10.1002/jgrd.50783, 2013.

5 Osthoff, H. D., Roberts, J. M., Ravishankara, A. R., Williams, E. J., Lerner, B. M., Sommariva, R., Bates, T. S., Coffman, D., Quinn, P. K., Dibb, J. E., Stark, H., Burkholder, J. B., Talukdar, R. K., Meagher, J., Fehsenfeld, F. C., and Brown, S. S.: High levels of nitryl chloride in the polluted subtropical marine boundary layer, *Nat. Geosci.*, 1, 324–328, 2008.

Papadimitriou, V. C., Karafas, E. S., Gierczak, T., and Burkholder, J. B.: CH<sub>3</sub>CO + O<sub>2</sub> + M (M = He, N<sub>2</sub>) reaction rate coefficient measurements and implications for the OH radical product yield, *J. Phys. Chem. A*, 119, 7481–7497, doi:10.1021/acs.jpca.5b00762, 2015.

Parrish, D. D. and Buhr, M. P.: Measurement challenges of nitrogen species in the atmosphere, in: *Advances in Chemistry*, American Chemical Society, Washington, DC, 243–273, 1993.

15 Paul, D., Furgeson, A., and Osthoff, H. D.: Measurements of total peroxy and alkyl nitrate abundances in laboratory-generated gas samples by thermal dissociation cavity ring-down spectroscopy, *Rev. Sci. Instrum.*, 80, 114101, doi:10.1063/1.3258204, 2009.

Perring, A. E., Pusede, S. E., and Cohen, R. C.: An observational perspective on the atmospheric impacts of alkyl and multifunctional nitrates on ozone and secondary organic aerosol, *Chem. Rev.*, 113, 5848–5870, doi:10.1021/cr300520x, 2013.

20 Phillips, G. J., Tang, M. J., Thieser, J., Brickwedde, B., Schuster, G., Bohn, B., Lelieveld, J., and Crowley, J. N.: Significant concentrations of nitryl chloride observed in rural continental Europe associated with the influence of sea salt chloride and anthropogenic emissions, *Geophys. Res. Lett.*, 39, L10811, doi:10.1029/2012GL051912, 2012.

Phillips, G. J., Pouvesle, N., Thieser, J., Schuster, G., Axinte, R., Fischer, H., Williams, J., Lelieveld, J., and Crowley, J. N.: Peroxyacetyl nitrate (PAN) and peroxyacetic acid (PAA) measurements by iodide chemical ionisation mass spectrometry: first analysis of results in the boreal forest and implications for the measurement of PAN fluxes, *Atmos. Chem. Phys.*, 13, 1129–1139, doi:10.5194/acp-13-1129-2013, 2013.

30 Pöhler, D., Vogel, L., Friess, U., and Platt, U.: Observation of halogen species in the Amundsen Gulf, Arctic, by active long-path differential optical absorption spectroscopy, *P. Natl. Acad. Sci. USA*, 107, 6582–6587, doi:10.1073/pnas.0912231107, 2010.

Ridley, B. A., Shetter, J. D., Walega, J. G., Madronich, S., Elsworth, C. M., Grahek, F. E., Fehsenfeld, F. C., Norton, R. B., Parrish, D. D., Hübler, G., Buhr, M., Williams, E. J., All-

TD-CRDS for NO<sub>2</sub>,  
RO<sub>2</sub>NO<sub>2</sub> and RONO<sub>2</sub>

J. Thieser et al.

Title Page

Abstract

Introduction

Conclusions

References

Tables

Figures



Back

Close

Full Screen / Esc

Printer-friendly Version

Interactive Discussion



- wine, E. J., and Westberg, H. H.: The behavior of some organic nitrates at Boulder and Niwot Ridge, Colorado, *J. Geophys. Res.*, 95, 13949–13961, 1990.
- Roberts, J. M.: The atmospheric chemistry of organic nitrates, *Atmos. Environ. A-Gen.*, 24, 243–287, doi:10.1016/0960-1686(90)90108-y, 1990.
- 5 Roberts, J. M., Jobson, B. T., Kuster, W., Goldan, P., Murphy, P., Williams, E., Frost, G., Riemer, D., Apel, E., Stroud, C., Wiedinmyer, C., and Fehsenfeld, F.: An examination of the chemistry of peroxy-carboxylic nitric anhydrides and related volatile organic compounds during Texas Air Quality Study 2000 using ground-based measurements, *J. Geophys. Res.-Atmos.*, 108, 4495, doi:10.1029/2003jd003383, 2003.
- 10 Roiger, A., Aufmhoff, H., Stock, P., Arnold, F., and Schlager, H.: An aircraft-borne chemical ionization – ion trap mass spectrometer (CI-ITMS) for fast PAN and PPN measurements, *Atmos. Meas. Tech.*, 4, 173–188, doi:10.5194/amt-4-173-2011, 2011.
- Rosen, R. S., Wood, E. C., Wooldridge, P. J., Thornton, J. A., Day, D. A., Kuster, W., Williams, E. J., Jobson, B. T., and Cohen, R. C.: Observations of total alkyl nitrates during Texas Air Quality Study 2000: implications for O<sub>3</sub> and alkyl nitrate photochemistry, *J. Geophys. Res.-Atmos.*, 109, D07303, doi:10.1029/2003jd004227, 2004.
- 15 Rothman, L. S., Gordon, I. E., Babikov, Y., Barbe, A., Benner, D. C., Bernath, P. F., Birk, M., Bizzocchi, L., Boudon, V., Brown, L. R., Campargue, A., Chance, K., Cohen, E. A., Coudert, L. H., Devi, V. M., Drouin, B. J., Fayt, A., Flaud, J. M., Gamache, R. R., Harrison, J. J., Hartmann, J. M., Hill, C., Hodges, J. T., Jacquemart, D., Jolly, A., Lamouroux, J., Le Roy, R. J., Li, G., Long, D. A., Lyulin, O. M., Mackie, C. J., Massie, S. T., Mikhailenko, S., Mueller, H. S. P., Naumenko, O. V., Nikitin, A. V., Orphal, J., Perevalov, V., Perrin, A., Polovtseva, E. R., Richard, C., Smith, M. A. H., Starikova, E., Sung, K., Tashkun, S., Tennyson, J., Toon, G. C., Tyuterev, V. G., and Wagner, G.: The HITRAN2012 molecular spectroscopic database, *J. Quant. Spectrosc. Ra.*, 130, 4–50, doi:10.1016/j.jqsrt.2013.07.002, 2013.
- 20 Ryerson, T. B., Williams, E. J., and Fehsenfeld, F. C.: An efficient photolysis system for fast-response NO<sub>2</sub> measurements, *J. Geophys. Res.-Atmos.*, 105, 26447–26461, doi:10.1029/2000jd900389, 2000.
- Schneider, M. and Ballschmiter, K.: C<sub>3</sub>–C<sub>14</sub> alkyl nitrates in remote South Atlantic air, *Chemosphere*, 38, 233–244, 1999.
- 30 Schuster, G., Labazan, I., and Crowley, J. N.: A cavity ring down/cavity enhanced absorption device for measurement of ambient NO<sub>3</sub> and N<sub>2</sub>O<sub>5</sub>, *Atmos. Meas. Tech.*, 2, 1–13, doi:10.5194/amt-2-1-2009, 2009.

TD-CRDS for NO<sub>2</sub>,  
RO<sub>2</sub>NO<sub>2</sub> and RONO<sub>2</sub>

J. Thieser et al.

Title Page

Abstract

Introduction

Conclusions

References

Tables

Figures



Back

Close

Full Screen / Esc

Printer-friendly Version

Interactive Discussion



- Singh, H. B. and Hanst, P. L.: Peroxyacetyl nitrate (PAN) in the unpolluted atmosphere: an important reservoir for nitrogen oxides, *Geophys. Res. Lett.*, 8, 941–944, 1981.
- Singh, H. B., Herlth, D., Kolyer, R., Salas, L., Bradshaw, J. D., Sandholm, S. T., Davis, D. D., Crawford, J., Kondo, Y., Koike, M., Talbot, R., Gregory, G. L., Sachse, G. W., Browell, E., Blake, D. R., Rowland, F. S., Newell, R., Merrill, J., Heikes, B., Liu, S. C., Crutzen, P. J., and Kanakidou, M.: Reactive nitrogen and ozone over the western Pacific: Distribution, partitioning, and sources, *J. Geophys. Res.*, 101, 1793–1808, 1996.
- Slusher, D. L., Huey, L. G., Tanner, D. J., Chen, G., Davis, D. D., Buhr, M., Nowak, J. B., Eisele, F. L., Kosciuch, E., Mauldin, R. L., Lefer, B. L., Shetter, R. E., and Dibb, J. E.: Measurements of pernitric acid at the South Pole during ISCAT 2000, *Geophys. Res. Lett.*, 29, 2011, doi:10.1029/2002gl015703, 2002.
- Suitters, M.: Long Path DOAS: the PARADE campaign, mode mixing and light source comparisons, Master Thesis, Institut for Environmental Physics, Heidelberg, 2012.
- Talukdar, R. K., Burkholder, J. B., Schmoltner, A. M., Roberts, J. M., Wilson, R. R., and Ravishankara, A. R.: Investigation of the loss processes for peroxyacetyl nitrate in the atmosphere – UV photolysis and reaction with OH, *J. Geophys. Res.-Atmos.*, 100, 14163–14173, doi:10.1029/95jd00545, 1995.
- Talukdar, R. K., Herndon, S. C., Burkholder, J. B., Roberts, J. M., and Ravishankara, A. R.: Atmospheric fate of several alkyl nitrates.1. Rate coefficients of the reactions alkyl nitrates with isotopically labelled hydroxyl radicals, *J. Chem. Soc. Faraday T.*, 93, 2787–2796, 1997.
- Tang, M. J., Thieser, J., Schuster, G., and Crowley, J. N.: Kinetics and mechanism of the heterogeneous reaction of N<sub>2</sub>O<sub>5</sub> with mineral dust particles, *Phys. Chem. Chem. Phys.*, 14, 8551–8561, 2012.
- Thaler, R. D., Mielke, L. H., and Osthoff, H. D.: Quantification of nitryl chloride at part per trillion mixing ratios by thermal dissociation cavity ring-down spectroscopy, *Anal. Chem.*, 83, 2761–2766, doi:10.1021/ac200055z, 2011.
- Thornton, J. A., Kercher, J. P., Riedel, T. P., Wagner, N. L., Cozic, J., Holloway, J. S., Dube, W. P., Wolfe, G. M., Quinn, P. K., Middlebrook, A. M., Alexander, B., and Brown, S. S.: A large atomic chlorine source inferred from mid-continental reactive nitrogen chemistry, *Nature*, 464, 271–274, doi:10.1038/nature08905, 2010.
- Trainer, M., Buhr, M. P., Curran, C. M., Fehsenfeld, F. C., Hsie, E. Y., Liu, S. C., Norton, R. B., Parrish, D. D., Williams, E. J., Gandrud, B. W., Ridley, B. A., Shetter, J. D., Allwine, E. J.,

TD-CRDS for NO<sub>2</sub>,  
RO<sub>2</sub>NO<sub>2</sub> and RONO<sub>2</sub>

J. Thieser et al.

Title Page

Abstract

Introduction

Conclusions

References

Tables

Figures



Back

Close

Full Screen / Esc

Printer-friendly Version

Interactive Discussion



and Westberg, H. H.: Observations and modeling of the reactive nitrogen photochemistry at a rural site, *J. Geophys. Res.*, 96, 3045–3063, 1991.

Tyndall, G. S., Staffelbach, T. A., Orlando, J. J., and Calvert, J. G.: Rate coefficients for the reactions of OH radicals with methylglyoxal and acetaldehyde, *Int. J. Chem. Kinet.*, 27, 1009–1020, 1995.

Voigt, S., Orphal, J., and Burrows, J. P.: The temperature and pressure dependence of the absorption cross-sections of NO<sub>2</sub> in the 250–800 nm region measured by Fourier-transform spectroscopy, *J. Photoch. Photobio. A*, 149, 1–7, doi:10.1016/s1010-6030(01)00650-5, 2002.

Volkamer, R., Molina, L. T., Molina, M. J., Shirley, T., and Brune, W. H.: DOAS measurement of glyoxal as an indicator for fast VOC chemistry in urban air, *Geophys. Res. Lett.*, 32, L08806, doi:10.1029/2005gl022616, 2005a.

Volkamer, R., Spietz, P., Burrows, J., and Platt, U.: High-resolution absorption cross-section of glyoxal in the UV-vis and IR spectral ranges, *J. Photoch. Photobio. A*, 172, 35–46, doi:10.1016/j.jphotochem.2004.11.011, 2005b.

Wagner, N. L., Riedel, T. P., Roberts, J. M., Thornton, J. A., Angevine, W. M., Williams, E. J., Lerner, B. M., Vlasenko, A., Li, S. M., Dube, W. P., Coffman, D. J., Bon, D. M., de Gouw, J. A., Kuster, W. C., Gilman, J. B., and Brown, S. S.: The sea breeze/land breeze circulation in Los Angeles and its influence on nitril chloride production in this region, *J. Geophys. Res.-Atmos.*, 117, D00V24, doi:10.1029/2012jd017810, 2012.

Warneck, P. and Zerbach, T.: Synthesis of peroxyacetyl nitrate in air by acetone photolysis, *Environ. Sci Technol.*, 26, 74–79, 1992.

Williams, J., Roberts, J. M., Fehsenfeld, F. C., Bertman, S. B., Buhr, M. P., Goldan, P. D., Hubler, G., Kuster, W. C., Ryerson, T. B., Trainer, M., and Young, V.: Regional ozone from biogenic hydrocarbons deduced from airborne measurements of PAN, PPN, and MPAN, *Geophys. Res. Lett.*, 24, 1099–1102, 1997.

Wolfe, G. M., Thornton, J. A., Yatavelli, R. L. N., McKay, M., Goldstein, A. H., LaFranchi, B., Min, K.-E., and Cohen, R. C.: Eddy covariance fluxes of acyl peroxy nitrates (PAN, PPN and MPAN) above a Ponderosa pine forest, *Atmos. Chem. Phys.*, 9, 615–634, doi:10.5194/acp-9-615-2009, 2009.

Wooldrige, P. J., Perring, A. E., Bertram, T. H., Flocke, F. M., Roberts, J. M., Singh, H. B., Huey, L. G., Thornton, J. A., Wolfe, G. M., Murphy, J. G., Fry, J. L., Rollins, A. W., LaFranchi, B. W., and Cohen, R. C.: Total Peroxy Nitrates (ΣPNs) in the atmosphere: the

Thermal Dissociation-Laser Induced Fluorescence (TD-LIF) technique and comparisons to speciated PAN measurements, *Atmos. Meas. Tech.*, 3, 593–607, doi:10.5194/amt-3-593-2010, 2010.

5 Yin-Nan, L., Xianliang, Z., and Hallock, K.: Atmospheric carbonyl compounds at a rural southeastern United States site, *J. Geophys. Res.*, 100, 25933–25944, 1995.

Zheng, W., Flocke, F. M., Tyndall, G. S., Swanson, A., Orlando, J. J., Roberts, J. M., Huey, L. G., and Tanner, D. J.: Characterization of a thermal decomposition chemical ionization mass spectrometer for the measurement of peroxy acyl nitrates (PANs) in the atmosphere, *Atmos. Chem. Phys.*, 11, 6529–6547, doi:10.5194/acp-11-6529-2011, 2011.

## AMTD

8, 11533–11596, 2015

### TD-CRDS for NO<sub>2</sub>, RO<sub>2</sub>NO<sub>2</sub> and RONO<sub>2</sub>

J. Thieser et al.

Title Page

Abstract

Introduction

Conclusions

References

Tables

Figures



Back

Close

Full Screen / Esc

Printer-friendly Version

Interactive Discussion



TD-CRDS for  $\text{NO}_2$ ,  
 $\text{RO}_2\text{NO}_2$  and  $\text{RONO}_2$ 

J. Thieser et al.

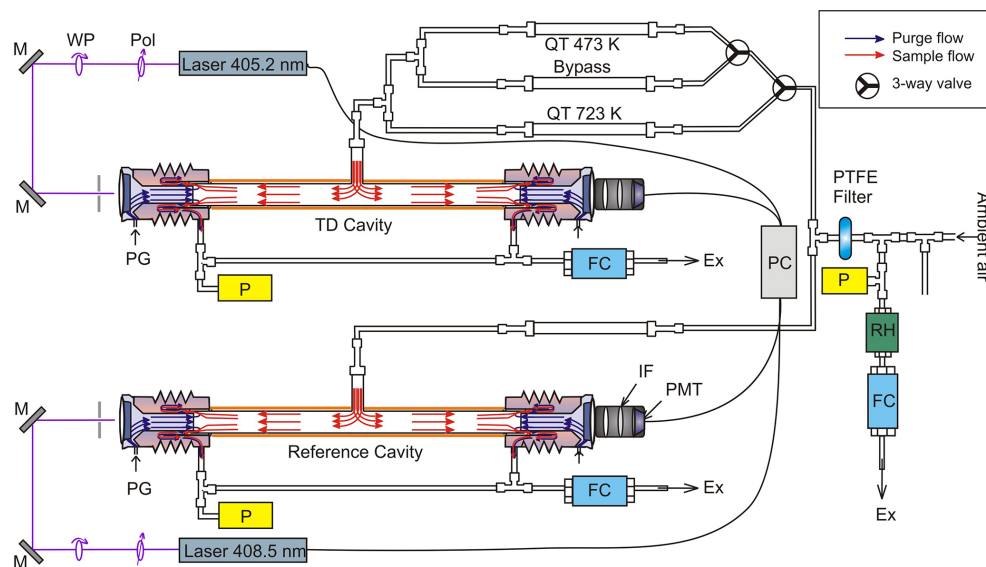


**Figure 1.** Schematic diagram of the two cavities (reference and TD) and associated inlets (quartz tubes at ambient temperature, 473 or 723 K). The reference cavity samples continuously via a quartz tube at ambient temperature, the TD-cavity samples sequentially from quartz tubing at ambient temperature, 473 or 723 K. Both cavities are held at 308 K and at constant pressure (usually 800 mbar). M = mirror, WP = quarter-wave plate, Pol = polariser, QT = quartz tubing, P = pressure transducer, FC = mass flow controller, PC = computer, RH = relative humidity and temperature sensor, IF = interference filter, PMT = photomultiplier, PG = purge gas, Ex = exhaust.

TD-CRDS for NO<sub>2</sub>,  
RO<sub>2</sub>NO<sub>2</sub> and RONO<sub>2</sub>

J. Thieser et al.

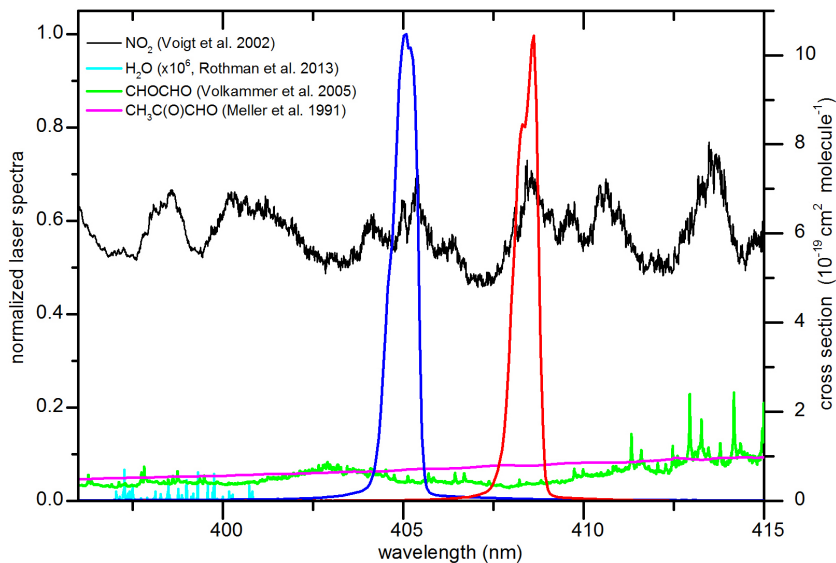


**Figure 2.** Laser emission spectrum (left y axis) measured in the reference cavity (blue) and the TD-cavity (red). The absorption spectra (Voigt et al., 2002; Meller et al., 1991; Volkamer et al., 2005b; Rothman et al., 2013) are associated with the right y axis. The H<sub>2</sub>O spectrum is scaled by a factor  $1 \times 10^6$ .

[Title Page](#)[Abstract](#)[Introduction](#)[Conclusions](#)[References](#)[Tables](#)[Figures](#)[◀](#)[▶](#)[◀](#)[▶](#)[Back](#)[Close](#)[Full Screen / Esc](#)[Printer-friendly Version](#)[Interactive Discussion](#)



TD-CRDS for  $\text{NO}_2$ ,  
 $\text{RO}_2\text{NO}_2$  and  $\text{RONO}_2$ 

J. Thieser et al.

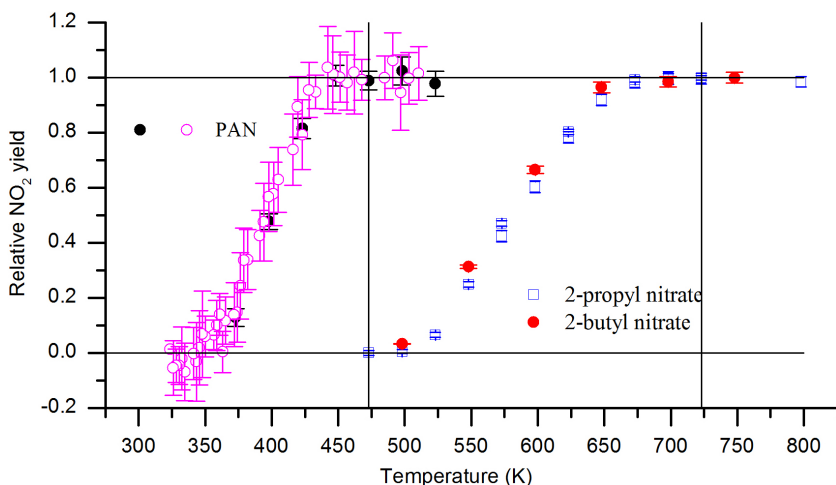


**Figure 3.** Efficiency of thermal dissociation of PAN and the ANs 2-propylnitrate and 2-butylnitrate. PAN ( $\approx 500$  pptv) was formed by the photolysis of acetone/ $\text{NO}$ /air sample (see text for details). The purple and black data points were measured before and after a campaign ( $\approx 2$  months separation in time). The ANs were available as diluted samples (several ppmv) in air which were diluted to  $\approx 10$  ppbv for these tests. The vertical lines indicate the nominal oven temperatures finally used.

[Title Page](#)[Abstract](#)[Introduction](#)[Conclusions](#)[References](#)[Tables](#)[Figures](#)[◀](#)[▶](#)[◀](#)[▶](#)[Back](#)[Close](#)[Full Screen / Esc](#)[Printer-friendly Version](#)[Interactive Discussion](#)

TD-CRDS for  $\text{NO}_2$ ,  
 $\text{RO}_2\text{NO}_2$  and  $\text{RONO}_2$ 

J. Thieser et al.

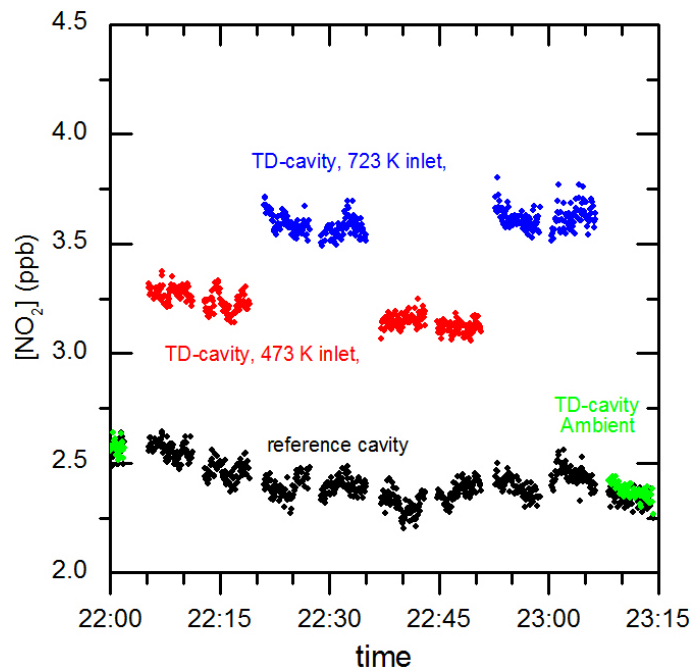


**Figure 4.** Example of a typical measurement cycle (showing raw data) when sampling ambient air. The black data points are the continuously measured  $\text{NO}_2$  mixing ratios measured by the reference cavity. The green, red and blue data points were recorded in the TD-cavity when sampling from the inlets at ambient, 473 and 723 K, respectively.

[Title Page](#)[Abstract](#)[Introduction](#)[Conclusions](#)[References](#)[Tables](#)[Figures](#)[Back](#)[Close](#)[Full Screen / Esc](#)[Printer-friendly Version](#)[Interactive Discussion](#)

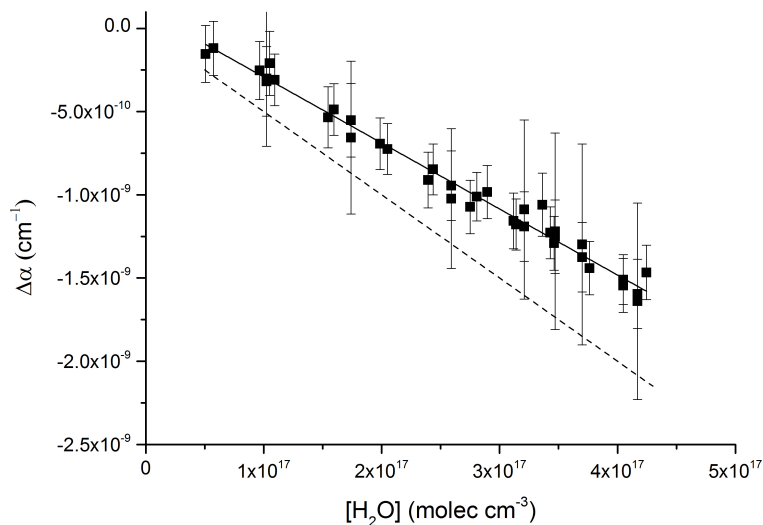


**Figure 5.** Determination of the scattering cross-section of H<sub>2</sub>O at 405 nm.  $\Delta\alpha$  is the change in measured extinction when H<sub>2</sub>O is added to dry air ( $\Delta\alpha = \alpha(\text{RH} = 0) - \alpha(\text{RH} > 0)$ ). The dashed line is the calculated value of  $\Delta\alpha$  when using the difference in scattering cross sections in dry and humid air reported by Fuchs et al. (2009).

[Title Page](#)[Abstract](#)[Introduction](#)[Conclusions](#)[References](#)[Tables](#)[Figures](#)[◀](#)[▶](#)[◀](#)[▶](#)[Back](#)[Close](#)[Full Screen / Esc](#)[Printer-friendly Version](#)[Interactive Discussion](#)

TD-CRDS for  $\text{NO}_2$ ,  
 $\text{RO}_2\text{NO}_2$  and  $\text{RONO}_2$ 

J. Thieser et al.

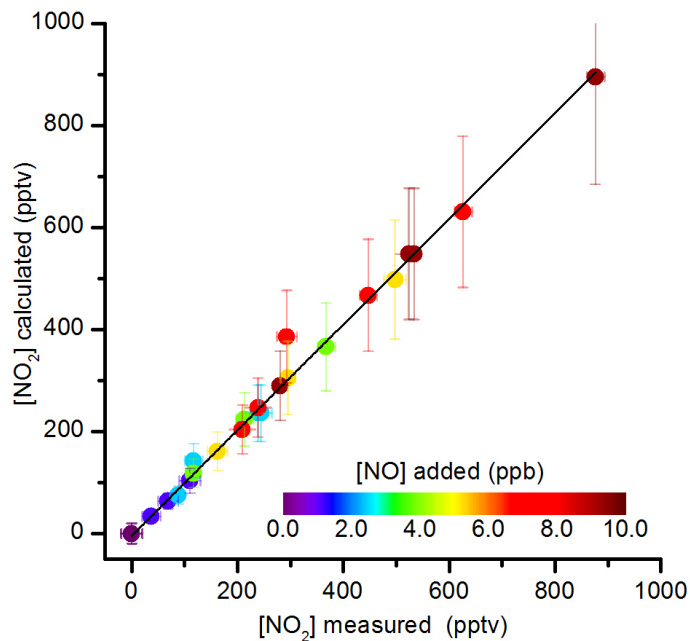


**Figure 6.**  $\text{NO}_2$  formation in the reaction of  $\text{O}_3$  with  $\text{NO}$  in the inlet (in this case at ambient temperature), and reference cavity (at 308 K) and connecting tubing. The error bars on the calculated  $\text{NO}_2$  formed are derived from the  $\sim 20\%$  error in the rate coefficient given for the rate coefficient (Atkinson et al., 2004). The fit to the data (black line) yields a slope of  $1.04 \pm 0.08$ .



TD-CRDS for  $\text{NO}_2$ ,  
 $\text{RO}_2\text{NO}_2$  and  $\text{RONO}_2$ 

J. Thieser et al.

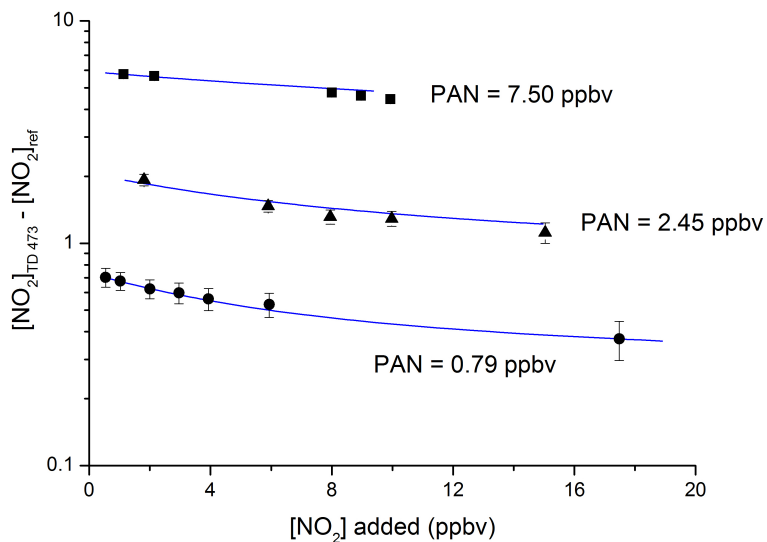


**Figure 7.** Measurements of the difference signal (TD cavity sampling from the 473 K inlet –  $\text{NO}_2$  reference cavity) with various amounts of  $\text{NO}_2$  added and at three different PAN concentrations (0.79, 2.45 and 7.50 ppbv). The error bars represent standard deviation and were derived by propagating errors in the  $\text{NO}_2$  signals in the TD and reference cavities. The blue lines are the results of numerical simulations as described in Sect. 2.1.7.

[Title Page](#)[Abstract](#)[Introduction](#)[Conclusions](#)[References](#)[Tables](#)[Figures](#)[◀](#)[▶](#)[◀](#)[▶](#)[Back](#)[Close](#)[Full Screen / Esc](#)[Printer-friendly Version](#)[Interactive Discussion](#)

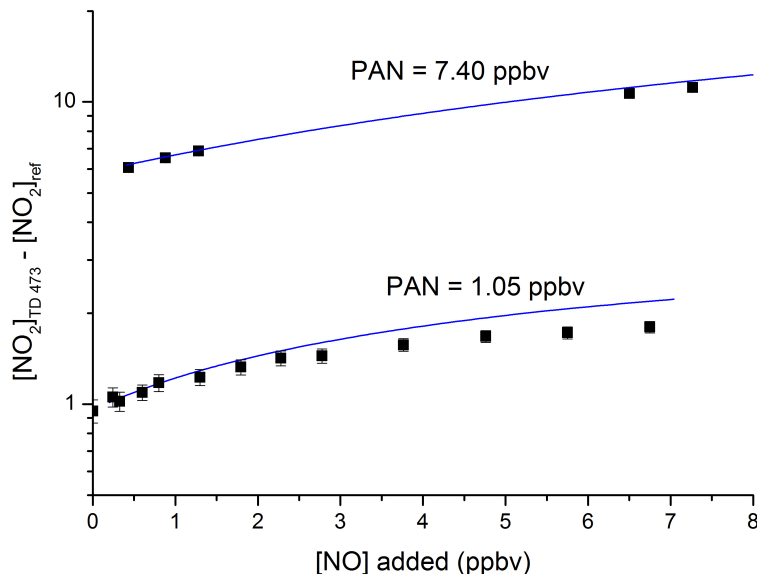


**Figure 8.** Measurements of the difference signal (TD cavity sampling from the 473 K inlet –  $\text{NO}_2$  reference cavity) with various amounts of  $\text{NO}$  added and at two different PAN concentrations (0.74 and 7.40 ppbv). The error bars represent standard deviation and were derived by propagating errors in the  $\text{NO}_2$  signals in the TD and reference cavities. The blue lines are numerical simulations as described in Sect. 2.1.7. The apparent worsening of the agreement between model and experiment at  $[\text{NO}] > 2.5$  ppbv is the result of drifts in the PAN mixing ratio during this experiment. By normalising to the PAN concentration (as in Fig. 10), the deviation disappears.

[Title Page](#)[Abstract](#)[Introduction](#)[Conclusions](#)[References](#)[Tables](#)[Figures](#)[◀](#)[▶](#)[◀](#)[▶](#)[Back](#)[Close](#)[Full Screen / Esc](#)[Printer-friendly Version](#)[Interactive Discussion](#)

TD-CRDS for NO<sub>2</sub>, RO<sub>2</sub>NO<sub>2</sub> and RONO<sub>2</sub>

J. Thieser et al.

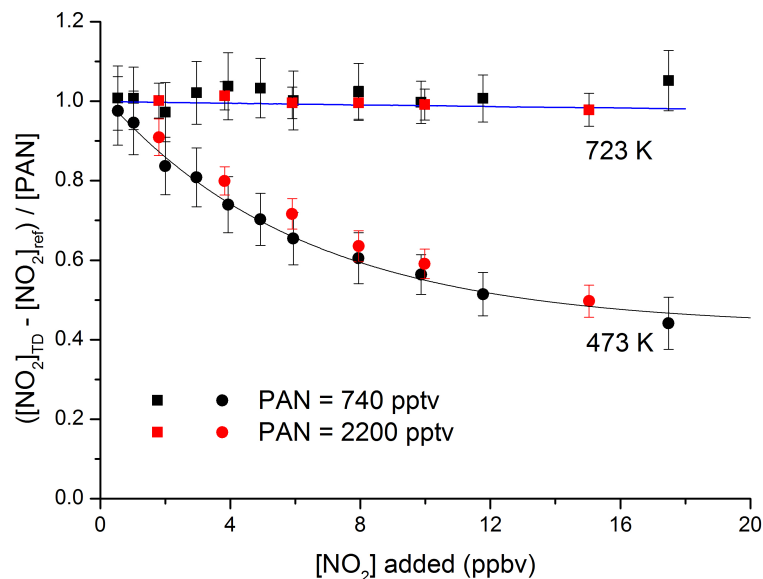


**Figure 9.** Measurements of the difference signal (TD cavity sampling from the 473 (squares) or 723 K inlet (circles) – NO<sub>2</sub> reference cavity) when adding different amounts of NO<sub>2</sub> to PAN samples (740 or 2200 pptv).  $[\text{NO}_2]_{\text{TD}}$  refers to the mixing ratio of NO<sub>2</sub> measured in the TD cavity sampling from either the 473 or 723 K inlet. The blue line is the model prediction of the effect of adding NO<sub>2</sub> to the 723 K inlet. The black line is an exponential fit to the NO<sub>2</sub> measured when sampling from the 473 K inlet and is added to guide the eye. The error bars represent standard deviation and were derived by propagating errors in the NO<sub>2</sub> signals in the TD and reference cavities.

Title Page

Abstract

Introduction

Conclusions

References

Tables

Figures

◀

▶

◀

▶

Back

Close

Full Screen / Esc

Printer-friendly Version

Interactive Discussion



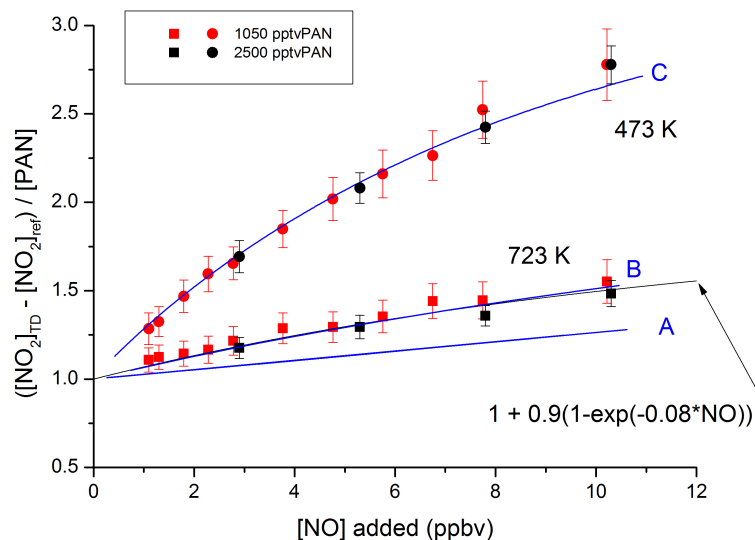


**Figure 10.** Measurements of the difference signal (TD cavity sampling from the 473 (squares) or 723 K inlet (circles) – NO<sub>2</sub> reference cavity) when adding different amounts of NO to PAN samples (1000 or 2500 pptv). [NO<sub>2</sub>]<sub>TD</sub> refers to the mixing ratio of NO<sub>2</sub> measured in the TD cavity sampling from either the 473 or 723 K inlet. The simulations (blue lines) labelled A and B are model predictions of the effect of adding NO<sub>2</sub> to the 723 K inlets using different rate constants for the rearrangement of CH<sub>3</sub>C(O)O<sub>2</sub> to CH<sub>2</sub>C(O)OH (see text for details). The simulation labelled C corresponds to the 473 K inlet. The error bars represent standard deviation and were derived by propagating errors in the NO<sub>2</sub> signals in the TD and reference cavities. The black lines are exponential fits to the data as described by the expressions given.

Title Page	
------------	--

Abstract	Introduction
----------	--------------

Conclusions	References
-------------	------------

Tables	Figures
--------	---------

◀	▶
---	---

◀	▶
---	---

Back	Close
------	-------

Full Screen / Esc
-------------------

Printer-friendly Version
--------------------------

Interactive Discussion
------------------------





TD-CRDS for  $\text{NO}_2$ ,  
 $\text{RO}_2\text{NO}_2$  and  $\text{RONO}_2$ 

J. Thieser et al.

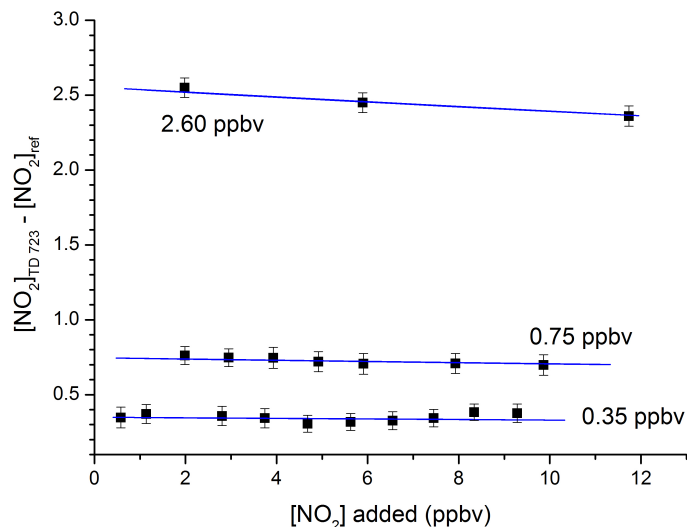


**Figure 11.** Measurements of the difference signal (TD cavity sampling from the 723 K inlet– $\text{NO}_2$  reference cavity) when adding different amounts of  $\text{NO}_2$  to 2-propyl nitrate samples (0.35, 0.75 or 2.6 ppbv). The error bars represent standard deviation and were derived by propagating errors in the  $\text{NO}_2$  signals in the TD and reference cavities. The blue lines show the model predictions of the effect of adding  $\text{NO}_2$  to the 723 K inlet as described in the text.

[Title Page](#)[Abstract](#)[Introduction](#)[Conclusions](#)[References](#)[Tables](#)[Figures](#)[◀](#)[▶](#)[◀](#)[▶](#)[Back](#)[Close](#)[Full Screen / Esc](#)[Printer-friendly Version](#)[Interactive Discussion](#)

TD-CRDS for  $\text{NO}_2$ ,  
 $\text{RO}_2\text{NO}_2$  and  $\text{RONO}_2$ 

J. Thieser et al.

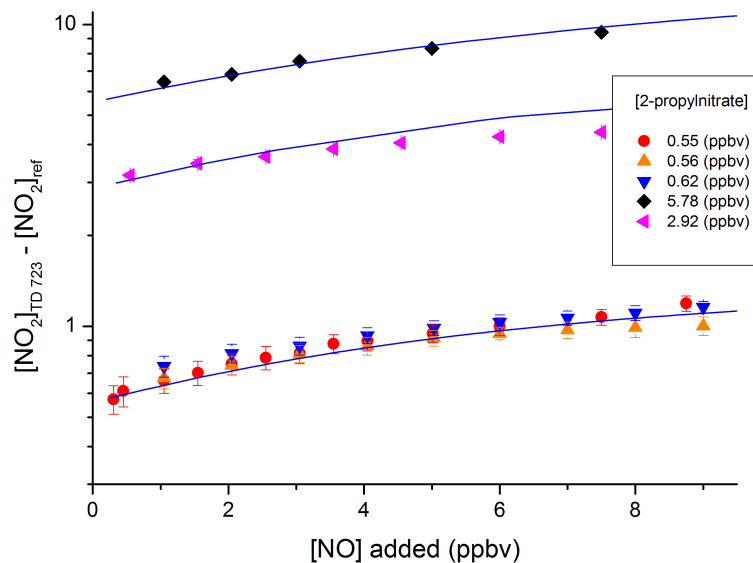


**Figure 12.** Measurements of the difference signal (TD cavity sampling from the 723 K inlet– $\text{NO}_2$  reference cavity) when adding different amounts of  $\text{NO}_2$  to 2-propyl nitrate samples (0.35, 0.56, 0.62, 2.92 or 5.78 ppbv). The sample with 0.62 ppbv 2-propyl nitrate also contained  $\sim 5$  ppbv of  $\text{NO}_2$ . The error bars represent standard deviation and were derived by propagating errors in the  $\text{NO}_2$  signals in the TD and reference cavities. The blue lines show the model predictions of the effect of adding  $\text{NO}$  to the 723 K inlet as described in the text.

Title Page

Abstract

Introduction

Conclusions

References

Tables

Figures

◀

▶

◀

▶

Back

Close

Full Screen / Esc

Printer-friendly Version

Interactive Discussion



TD-CRDS for  $\text{NO}_2$ ,  
 $\text{RO}_2\text{NO}_2$  and  $\text{RONO}_2$ 

J. Thieser et al.

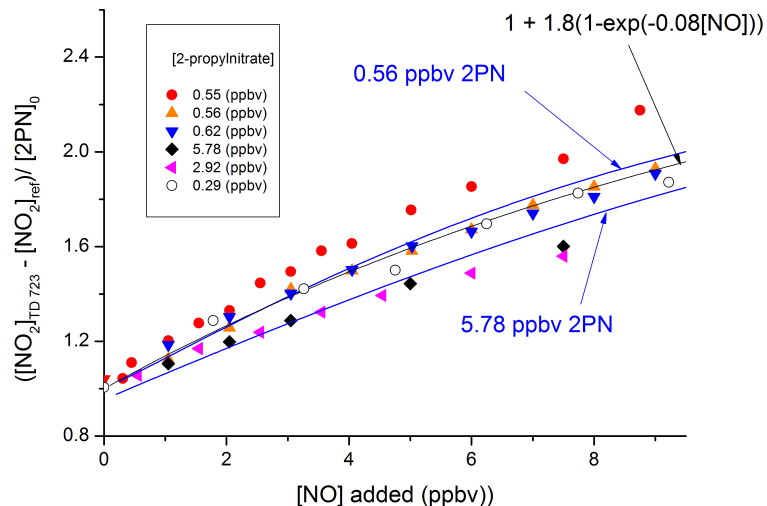


**Figure 13.** Relative change in difference signal ( $([\text{NO}_2]_{\text{TD } 723} - [\text{NO}_2]_{\text{ref}}) / [2\text{PN}]_0$ ) as a function of added NO for 6 different 2-propylnitrate (2PN) mixing ratios.  $[2\text{PN}]_0$  is the measured mixing ratio of 2-propylnitrate in the absence of added NO. The sample with 0.62 ppbv 2-propylnitrate also contained  $\sim 5$  ppbv of  $\text{NO}_2$ . The black line is defined by the expression  $([\text{NO}_2]_{\text{TD } 723} - [\text{NO}_2]_{\text{ref}}) / [2\text{PN}]_0 = 1 + 1.8 \times (1 - \exp(-0.08[\text{NO}]))$  where  $[\text{NO}]$  is the mixing ratio of NO in ppbv. The blue lines show model results with 0.56 and 5.7 ppbv 2-propylnitrate.

Title Page

Abstract

Introduction

Conclusions

References

Tables

Figures

◀

▶

◀

▶

Back

Close

Full Screen / Esc

Printer-friendly Version

Interactive Discussion



TD-CRDS for  $\text{NO}_2$ ,  
 $\text{RO}_2\text{NO}_2$  and  $\text{RONO}_2$ 

J. Thieser et al.

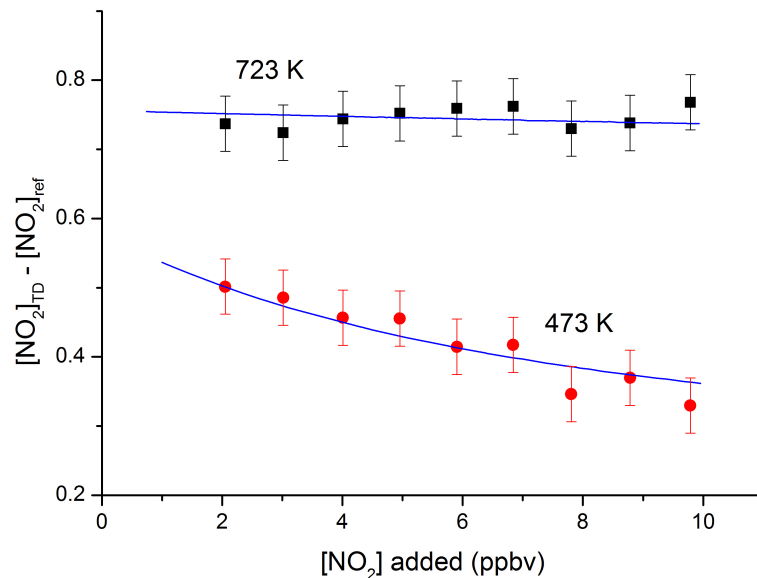


**Figure 14.** Dependence of  $([\text{NO}_2]_{\text{TD}473} - [\text{NO}_2]_{\text{ref}})$  and  $([\text{NO}_2]_{\text{TD}723} - [\text{NO}_2]_{\text{ref}})$  on added  $\text{NO}_2$  in the presence of PAN (0.53 ppbv) and AN (0.19 ppbv). The error bars represent standard deviation and were derived by propagating errors in the  $\text{NO}_2$  signals in the TD and reference cavities. The blue lines show the model results as described in the text.

[Title Page](#)[Abstract](#)[Introduction](#)[Conclusions](#)[References](#)[Tables](#)[Figures](#)[◀](#)[▶](#)[◀](#)[▶](#)[Back](#)[Close](#)[Full Screen / Esc](#)[Printer-friendly Version](#)[Interactive Discussion](#)

TD-CRDS for  $\text{NO}_2$ ,  
 $\text{RO}_2\text{NO}_2$  and  $\text{RONO}_2$ 

J. Thieser et al.

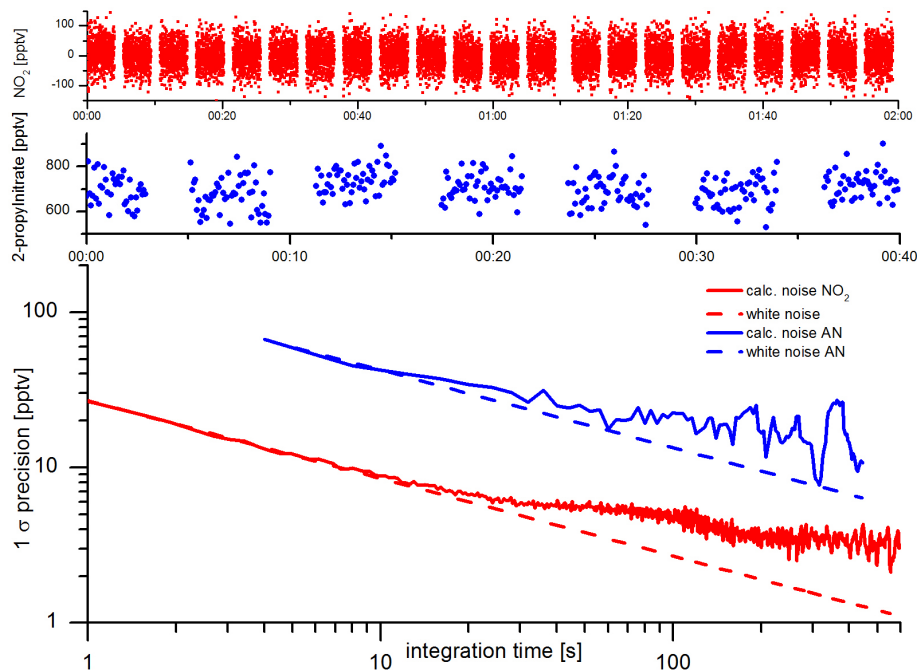


**Figure 15.** The upper panel (red data points) displays a time series of raw  $\text{NO}_2$  data (5 s intervals) when sampling zero air. The middle panel (blue data points) shows a series of measurements when sampling a constant flow of 2-propylnitrate ( $\sim 700$  pptv) from the 723 K inlet. The lower panel is an Allan deviation plot showing the dependence of the measurement precision ( $1\sigma$ ) on the signal integration time in the reference cavity (red curve) and TD cavity (blue curve). The dashed lines represent precision expected for random noise.



TD-CRDS for  $\text{NO}_2$ ,  
 $\text{RO}_2\text{NO}_2$  and  $\text{RONO}_2$ 

J. Thieser et al.

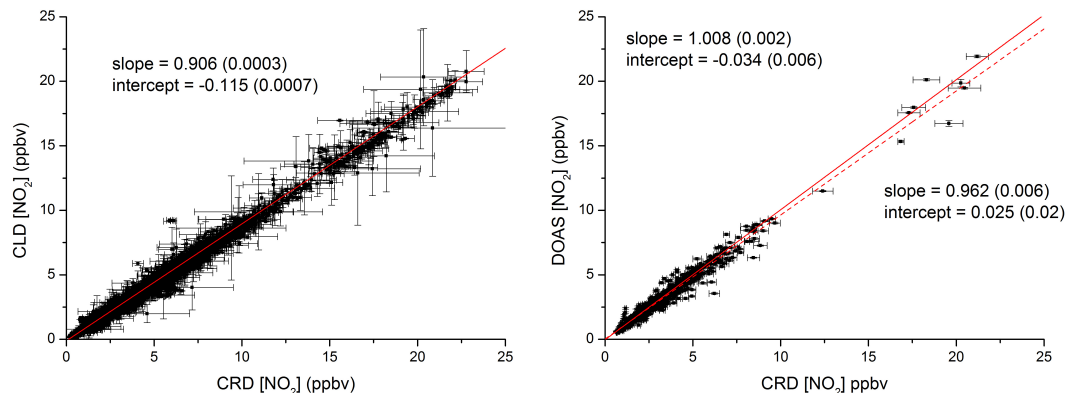


**Figure 16.** Comparison of  $\text{NO}_2$  data (reference cavity) from the TD-CRDS with two established instruments. Left panel: chemiluminescence detector (CLD), 1 min data averages. Right panel: long path differential absorption spectrometer (DOAS), 10 min data averages. The red, solid lines are weighted bivariate fits considering reported standard deviations for both instruments, the dashed line is an unweighted fit. For the DOAS comparison only data were used for which the CRDS indicated standard deviations of less than 5 % (over 10 min intervals).

[Title Page](#)[Abstract](#)[Introduction](#)[Conclusions](#)[References](#)[Tables](#)[Figures](#)[◀](#)[▶](#)[◀](#)[▶](#)[Back](#)[Close](#)[Full Screen / Esc](#)[Printer-friendly Version](#)[Interactive Discussion](#)

TD-CRDS for  $\text{NO}_2$ ,  
 $\text{RO}_2\text{NO}_2$  and  $\text{RONO}_2$ 

J. Thieser et al.

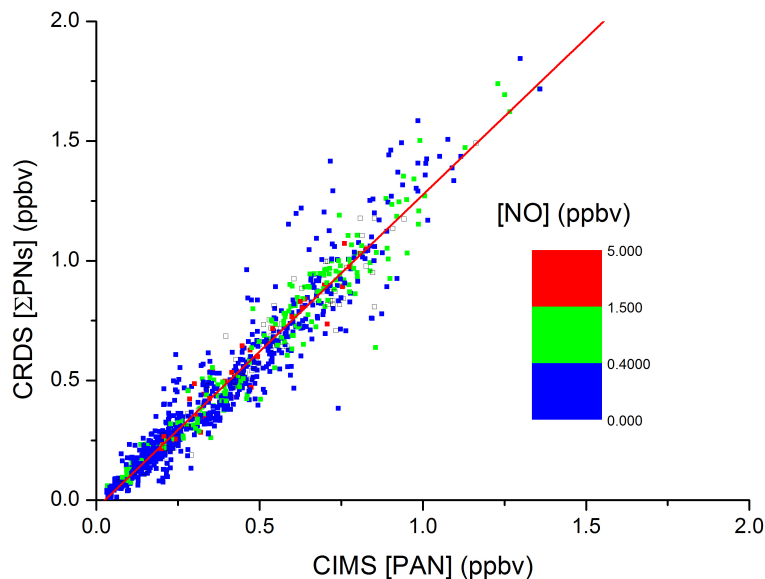


**Figure 17.** PARADE data: comparison of PAN derived by the TD-CIMS with the TD-CRDS measurement of  $\Sigma\text{PNs}$ . The  $\Sigma\text{PNs}$  data have been corrected as described in the text. The data is colour-coded according to  $[\text{NO}]$  mixing ratios.

[Title Page](#)[Abstract](#)[Introduction](#)[Conclusions](#)[References](#)[Tables](#)[Figures](#)[◀](#)[▶](#)[◀](#)[▶](#)[Back](#)[Close](#)[Full Screen / Esc](#)[Printer-friendly Version](#)[Interactive Discussion](#)

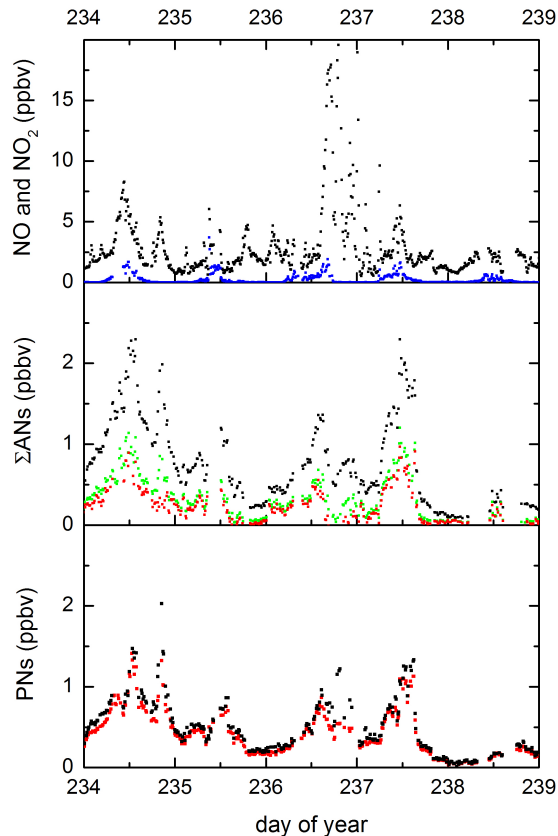


**Figure 18.** Time series of PARADE data over a 5 day period. The upper panel shows the  $\text{NO}_2$  mixing ratios measured in the reference cavity along with  $\text{NO}$  measured by the CLD. The central panel shows the TD cavity measurements when sampling from the 723 K inlet, the lower panel when sampling from the 450 K inlet. Black data points are uncorrected, the red data points include the corrections described in the text.

Title Page	
Abstract	Introduction
Conclusions	References
Tables	Figures
◀	▶
◀	▶
Back	Close
Full Screen / Esc	
Printer-friendly Version	
Interactive Discussion	

